Front. Earth Sci. 2020, 14(1): 90–109
https://doi.org/10.1007/s11707-018-0741-9

RESEARCH ARTICLE

Numerical modeling of the seasonal circulation in the coastal ocean of the Northern South China Sea

Yang DING[1], Zhigang YAO (✉)[2], Lingling ZHOU[2], Min BAO[3], Zhengchen ZANG[4]

1 Physical Oceanography Laboratory/CIMST, Ocean University of China and Qingdao National Laboratory for Marine Science and Technology, Qingdao 266100, China
2 College of Oceanic and Atmospheric Sciences, Ocean University of China, Qingdao 266100, China
3 State Key Laboratory of Satellite Ocean Environment Dynamics, Second Institute of Oceanography, State Oceanic Administration, Hangzhou 310012, China
4 Department of Oceanography and Coastal Sciences, Louisianan State University, Baton Rouge, LA 70803, USA

Abstract The Finite Volume Community Ocean Model (FVCOM) was adapted to the Northern South China Sea (NSCS) to investigate the seasonality of coastal circulation, as well as along-shelf and cross-shelf transport. In fall and winter, southwestward current dominates the NSCS shelf, while the current's direction shifts to northeast in summer. The circulation pattern in spring is more complicated: both southwestward and northeastward currents are detected on the NSCS shelf. The mean shelf circulation pattern in winter does not show the permanent counter-wind South China Sea Warm Current (SCSWC) along the 100–200 m isobaths. Meanwhile, the model results indicate a northeastward current flowing along 50–100 m isobaths in spring. Southwestward along-shelf transport varies from 0.30–1.93 Sv in fall and winter, and it redirects to northeast in summer ranging from 0.44–1.09 Sv. Onshore transport is mainly through the shelf break segment southeast of the Pearl River Estuary.

Keywords Northern South China Sea, coastal ocean, seasonal circulation, along-shelf and cross-shelf transport, Ocean model, FVCOM

1 Introduction

The Northern South China Sea (NSCS) is a marginal sea in the northwestern Pacific. It has a broad shelf extending from the Beibu Gulf to the southwest of Taiwan Strait (Fig. 1). The NSCS is dominated by the East Asian Monsoon system (Hu et al., 2000). In summer season the weak southwesterly wind dominates while in winter strong northeasterly wind prevails in the NSCS. The circulation on the NSCS shelf is forced by monsoons, tides, buoyancy forcing, topography, and open ocean processes such as Kuroshio through the Luzon Strait (Hu et al., 2000; Wang et al., 2014). Large river plumes, significant along-shelf and cross-shelf transport, upwelling and downwelling also greatly influence the current fields (Shu et al., 2018).

The shelf circulation pattern in the NSCS dominated by the above-mentioned physical processes contribute significantly to the transport of low-salinity water, sediment, and contaminants, and also impact the ecological environment in the shelf sea of NSCS (Chen et al., 2001; Su, 2004; Li et al., 2015; Meng et al., 2017). For example, the upwelling intensity in the coastal region associated with the alongshore currents in the NSCS (Wang et al., 2014) is able to influence the dissolved organic carbon (DOC) biogeochemistry (Álvarez-Salgado et al., 2001; Hill and Wheeler, 2002). The dynamics of dissolved inorganic nitrogen (DIN), dissolved inorganic phosphorus (DIP), and silicate ($Si(OH)_4$) on the NSCS shelf are controlled by the complicated hydrodynamic environment including large river plume and coastal upwelling (Han et al., 2012). Meng et al. (2017) also stated that the seasonal dynamics of the DOC in the NSCS shelf were primarily dominated by the regional circulation and cross-shelf transport. The spatial pattern of circulation over the NSCS shelf is mainly related to the NSCS shelf's topography that involves a wide shelf, a narrow strait (Qiongzhou Strait), and a large shallow gulf of Beibu Gulf (Shu et al., 2011a; Wang et al., 2014). While the upper layer circulation on the basin scale in the South China Sea (SCS) shows distinct seasonality due to monsoon activities (Wyrtki, 1961; Hu et al., 2000; Shu et al., 2018). Moreover, the Pearl River also contributes to the NSCS circulation (Su, 2004; Shu et al., 2011b, 2014).

Received May 27, 2018; accepted October 8, 2018

E-mail: yaozhigang@ouc.edu.cn

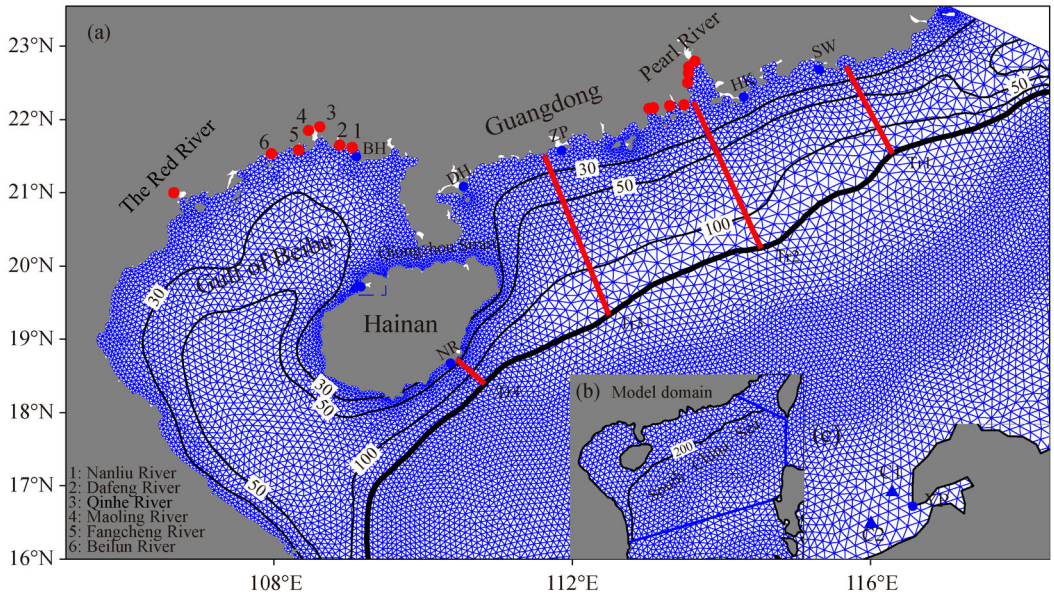

Fig. 1 (a) Map and model mesh (blue triangles) of the Northern South China Sea with depth contours (black lines) and locations of coastal tide gauge stations (blue dots): SW (Shanwei), HK (Hong Kong), ZP (Zhapo), DH (Donghai), BH (Beihai), and NR (Nanrong); tidal current stations (blue triangles); The red dots indicate the Pearl River, the Red River, and six smaller rivers along the northern coast of the Beibu Gulf. Thick black line denotes the 200 m isobath; Red lines denote cross-shelf transects where temperature, salinity and velocity are sampled. (b) Model domain with blue lines indicating the open boundaries. (c) Enlarged view of the tidal elevation and tidal current stations for the area with blue dashed lines in (a).

The freshwater discharge from the Pearl River ranges from ~4×10^3 m^3/s during winter to 2×10^4 m^3/s during summer (Wong et al., 2003; Chen et al., 2016). The Pearl River Estuary (PRE) links the river with the shelf in the NSCS. Under the northeasterly monsoon in winter and autumn, the freshwater around the PRE expands southwest along the coast, while the larger river plume spreads both southwestward and northeastward over the inner shelf when the monsoon turns to southwest (Shi et al., 2002; Su, 2004; Zu and Gan, 2015; Chen et al., 2017). The interactions between circulation around the PRE and the shelf circulation were intensively investigated by previous studies (Zu and Gan, 2015; Chen et al., 2016; Chen et al., 2017).

The Guangdong Coastal Current (GCC) and South China Sea Warm Current (SCSWC) dominate the coastal circulation system on the NSCS shelf (Hu et al., 2000; Wang et al., 2014; Ji et al., 2015). Previous studies reveal that the GCC flows westward in winter and eastward in summer (Fang et al., 1998; Hu et al., 2000; Su, 2004). Based on field measurements and numerical model, Bao et al. (2005) and Ding et al. (2017) conclude that the GCC west of the PRE flows southwest due to southwesterly monsoon wind. The SCSWC is northeastward over the shelf break off Guangdong and featured by counter-wind direction in winter (Guan and Chen, 1964; Qiu et al., 1985; Guan and Fang, 2006; Chiang et al., 2008). Numerous studies paid much attention to the characteristics and formation mechanism of the SCSWC in winter season since it was proposed (Liu and Su, 1993; Wang et al., 2011; Xie et al., 2015; Zhang et al., 2017). However, recent measurements based on eight current mooring stations over the NSCS in the 2006–2007 and 2009–2010 winters challenged the existence of the permanent SCSWC during wintertime (Li et al., 2014). Therefore, the permanent SCSWC during winter and its dynamic mechanism are still under debate.

Previous studies show that circulation in the Beibu Gulf is characterized by significant seasonal variation (Chern et al., 2010; Ding et al., 2013; Gao et al., 2017). In fall and winter, the cyclonic circulation dominates the entire gulf under northeasterly monsoon (Gao et al., 2017). The summer circulation pattern in the Beibu Gulf is still unclear mainly due to its complicated mechanisms (Gao et al., 2017). Several studies mentioned that the circulation in summer is anti-cyclonic (Wu et al., 1998; Sun et al., 2001), while other investigations argued that cyclonic circulation also exists in the Beibu Gulf during the summer season (Xia et al., 2001; Wu et al., 2008; Ding et al., 2013). The inconsistency between previous studies might due to the tides, water stratification, and interannual variations of southwesterly monsoon and fresh water discharge from the Red River (Ding et al., 2013; Gao et al., 2017).

A large number of field and model studies have contributed to the understanding of the seasonality of circulation in the SCS (Xu et al., 1982; Shaw and Chao, 1994; Wu et al., 1998; Cai et al., 2002; Xue et al., 2004; Xie et al., 2015; Liu and Gan, 2017). These studies

revealed the characteristics and driving forces of the circulation in the SCS and provided a remarkable SCS circulation pattern. We note that previous studies focused on the SCS circulation pattern mainly on the basin scale. Many studies investigated the deep ocean circulation of the SCS and interactions between the SCS and northwestern Pacific. There are some studies focused on the hydrodynamics over the shelf region of the NSCS based on numerical models. However, these studies paid more attention to the upwelling circulation along the coastal region on the NSCS shelf (Gan et al., 2009a, b, 2010, 2013, 2015; Wang et al., 2012, 2014; Lin et al., 2016). One should be aware that the water properties over continental shelves are distinctly different from that in the open ocean as continental shelves are featured by water mixing. Consequently, the circulation over the shelf region is influenced by both coastal and deep oceanic processes. For the NSCS, a broad continental shelf exists and the circulation over the shelf is rather complicated due to combined effects from topography, monsoon, freshwater discharge, extreme weather process (i.e., typhoons), and the deep ocean exchange process. A quantitive description and basic understanding of the circulation over the NSCS shelf can provide important information for the studies regarding biogeochemistry and ecosystems in the NSCS. Moreover, direct current measurements in the shallow waters of NSCS are rather rare, which hinders our understanding of the shelf dynamics in this region. Although more field observations needed to be carried out in the NSCS, our study try to explore the NSCS shelf circulation based on a regional ocean model, which provides valuable reference for the understanding the NSCS shelf circulation.

In this study, an 18-year (from 1995 to 2012) circulation hindcast based on a regional circulation model is performed to overcome the limitation of observations. We aim to obtain the seasonal variation of three-dimensional circulation and its spatial pattern in coastal NSCS. Shelf hydrodynamics and interaction between deep ocean and shallow shelf are comprehensively discussed herein. This paper is structured as follows. Section 2 describes the detailed information regarding ocean model configuration and model validation. Section 3 illustrates the seasonal pattern of circulation over the NSCS shelf and its three-dimensional characteristics. The along-shelf and cross-shelf transports are estimated in Section 4, which is followed by the conclusions in Section 5.

2 Ocean model

2.1 Model configuration

The coastal circulation simulation in this paper was performed based on the Finite Volume Community Ocean Model (FVCOM, version 3.2). Detailed references about this ocean model can be found in Chen et al. (2003, 2007a). FVCOM is a free-surface, hydrostatic, unstructured-grid, primitive-equation model that has been extensively adopted in regional studies (Lai et al., 2015; Ding et al., 2017; Xuan et al., 2017).

The model domain encompasses the NSCS shelf extending from 16°N to 23°N and from 105°E to 120°E (Fig. 1). The horizontal resolution ranges from 5 km along the coast to 30 km near the open boundaries. Vertically there are 30 terrain-following levels in total. Smagorinsky turbulent closure scheme and Mellor and Yamada level 2.5 (MY-2.5) are specified to resolve horizontal and vertical mixing, respectively (Smagorinsky, 1963; Mellor and Yamada, 1982). Detailed model parameters used in the simulation are shown in Table 1. A combination of bathymetry data obtained from sea chart of China coastal sea and topography derived from DBDB5 was adopted for the model depth. Driving forces of the model included real-time tidal forcing, fresh-water discharge, wind, air pressure, surface net heat flux and short-wave radiation, precipitation and evaporation, and open boundary conditions. We adopted reanalysis data of daily sea surface height (SSH), velocity, temperature, and salinity from the global HYCOM model (Bleck, 2002; Chassignet et al.,

Table 1 Model parameters used in the mode simulations

Model parameters	Values
Number of nodes	14,711
Number of triangles	28,577
External time step	8.0 s
Internal time step	80.0 s
Horizontal diffusion	Smagorinsky eddy parameterization method (Smagorinsky, 1963)
Vertical diffusion	Mellor and Yamada level 2.5 turbulent closure model (Mellor and Yamada, 1982)
Horizontal mixing coefficient (background value)	0.1
Horizontal Prandtl number	0.1
Vertical mixing coefficient (background value)	1.000E–5
Vertical Prandtl number	1.0
Bottom friction parametrization	Logarithmic bottom friction
Bottom roughness length scale	0.001
The attenuation depth for longer wavelength component of the shortwave irradiance	1.40
The attenuation depth for shorter wavelength component of the shortwave irradiance	6.30
Fraction of the total flux associated with the longerwavelength irradiance	0.78
Minimum bottom roughness value (background value)	0.0025
Number of CPU for parallelization	64

2007) from 1992 to 2012 to provide the lateral open boundary conditions for the model. Tidal forcing based on eight tidal constituents (M_2, S_2, N_2, K_1, O_1, Q_1, M_4, MS_4) obtained from TPXO 7.2 (Egbert and Erofeeva, 2002) was also applied along the open boundaries. In our simulations, clamped condition is used for the lateral open boundary conditions for zeta, *u*, *v*, temp and salinity. In FVCOM, the velocity is placed on the center of a triangle and scalar variables are placed on the vertex of a triangle. Therefore, we interpolated the HYCOM results to the center (e.g., current speed) and vertexes (sea level, temperature, and salinity) of the triangle mesh along the open boundary.

At the solid boundary, river discharge from Pearl River, the Red River, and six small rivers (Nanliu River, Dafeng River, Qinhe River, Maoling River, Fangcheng River and Beilun River, locations see Fig. 1) were included in the simulations. The monthly freshwater flux was obtained from Chen et al. (2012), Ding et al. (2013), and Gao et al. (2013). For the surface forcing, the hourly data were derived from National Center for Environmental Prediction (NCEP) Climate Forecast System Reanalysis (CFSR). A nudging method was applied to constrain the model simulated sea surface temperature (SST) and SSH. The assimilated sea surface temperature data were obtained from the satellite-derived SST data (NOAA High-resolution Blended Analysis of Daily SST, Reynolds et al., 2007). SSH was nudged back to the climatology derived from TOPEX/POSEIDON (T/P). The time period of the daily-mean SST and T/P data used for nudging ranges from October 1, 1992 to December 31, 2012. It should be kept in mind that the shelf region is characterized by strong tide and the T/P data is less accurate in shallow region than that in deep ocean. Therefore, SSH nudging was only applied to the region with depth > 1000 m. The initial conditions (i.e., temperature and salinity) were obtained from the HYCOM on October 1st, 1992. The simulation period was from October 1st, 1992 to December 31st, 2012. Since we initialized SSH and currents as zero, our simulations from 1992 to 1994 were treated as spin-up period and model results were analyzed from 1995 to 2012 (18 years). The time step was 8 seconds for barotropic mode and 80 seconds for the baroclinic mode, respectively.

2.2 Model-data comparison

2.2.1 *in-situ* measurements

The observed SSH at stations Zhapo (ZP, time range: 1975–1997), Beihai (BH, time range: 1975–1997), Shanwei (SW, time range: 1975–1997), and Hong Kong (HK, time range: 1962–2012) were downloaded from University of Hawaii Sea Level Center (UHSLC). The SSH at stations Donghai (DH, time range: 2006-03-01–2006-03-31), Nanrong (NR, 2007-08-01–2007-08-30), and Yangpu (YP, time range: 2010-03-01–2010-03-31) were provided by Ocean University of China (OUC). These observed SSH data are at hourly intervals. Data within one month's duration in different years were selected for comparison. It should be noted that nearly all the sea level data observed at the tide stations in the NSCS obtained from UHSLC are before year 1997. The long-time observations of sea level elevations from 1995 to 2012 are only available at station HK.

Direct long-term current observations were relatively limited in the NSCS. We only collected data from two current stations in this region. The current observations at station C1 and C2 were conducted on December 23, 2010 by OUC northwest of Hainan Island using Electromagnetic current meter for 30 hours. Besides, we digitized the field measurements of Zhang (2014) in different seasons to further calibrate our simulation results. Since the direct tidal current measurements are limited, we further obtained the tidal current ellipses data from the 1/30° China Sea tide model of the Oregon State University Tidal Inversion Software (OTIS model, Egbert and Erofeeva, 2002). The tidal current ellipse parameters of four main tidal constituents (M_2, S_2, K_1, and O_1) from the OTIS model are used to validate our model results.

To validate the model-simulated temperature and salinity, the climatology mean temperature and salinity field from SCS Physical Oceanographic Dataset (SCSPOD14, Zeng et al., 2016a) were adopted. The SCSPOD14 is comprises of monthly mean temperature and salinity built upon the World Ocean Database (WOD), Array for Real-time Geostrophic Oceanography (Argo) floats, and observed data from the South China Sea (SCS) Institute of Oceanography (SCSIO) for the period 1919–2014. The SCSPOD14 dataset focused on the region of the South China Sea, and the reliability of this dataset was confirmed by comparison with the World Ocean Atlas (WOA), and it has been used to study the hydrography in the SCS (Zeng et al., 2016b; Zeng and Wang, 2017).

2.2.2 Tidal elevations comparison

Figure 2 shows the comparison between observed and simulated hourly tidal elevations at seven tidal stations in the NSCS, whose locations are marked in Fig. 1. The simulated hourly time series of tidal elevations agreed well with the observations. The model captured the semi-diurnal (ZP, SW, DH, HK) and diurnal cycles (BH, NR, YP) of the tidal oscillations. The spring neap tides during one month at different stations were also resolved in the model simulation. The correlation coefficients between simulation and observations are higher than 0.89 except at station SW. However, differences between model-simulated and observed tidal elevations can be noted. The model overestimated the tidal amplitude at station BH, and YP and underestimated the amplitude at station ZP, DH, and HK. The discrepancies can be mainly attributed to the

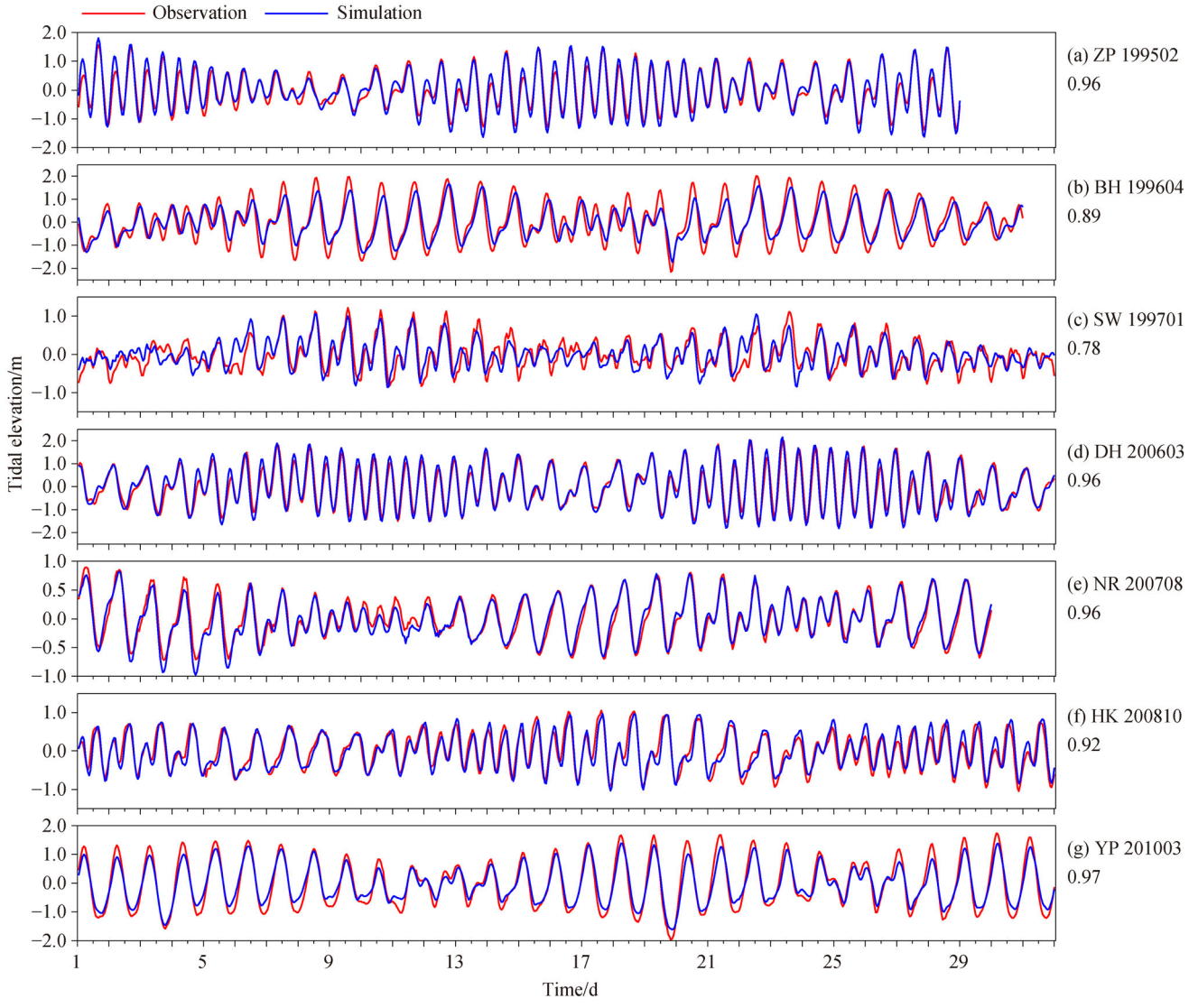

Fig. 2 Comparisons of simulated and observed hourly tidal elevations along the NSCS coast. The correlation coefficients (above with 95% confidence level) for each station are also shown in the figure.

topography and spatial resolution of the model, as some tide gauge stations locate inside small estuaries that the model cannot resolve.

2.2.3 Tidal currents and tidal ellipses comparison

The simulated depth-averaged tidal currents were compared with the observations at station C1 and C2 on December 23rd, 2010 (Fig. 3). The model results captured the tidal cycle of the diurnal tide at two stations. Figure 4 shows the comparison of the vertical-averaged tidal current ellipses of four main tidal components (M_2, S_2, K_1, and O_1) between the OTIS model and our model in the NSCS. The region with depth less than 200 m is shown. The model-simulated tidal current ellipse showed good agreement with the OTIS model. Both the OTIS model and our model

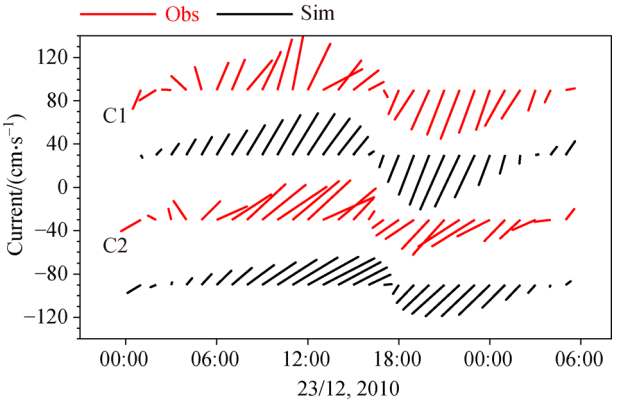

Fig. 3 Comparisons of modeled and observed hourly tidal currents at coastal stations C1 and C2 northwest of the Hainan Island (Fig. 1(c)).

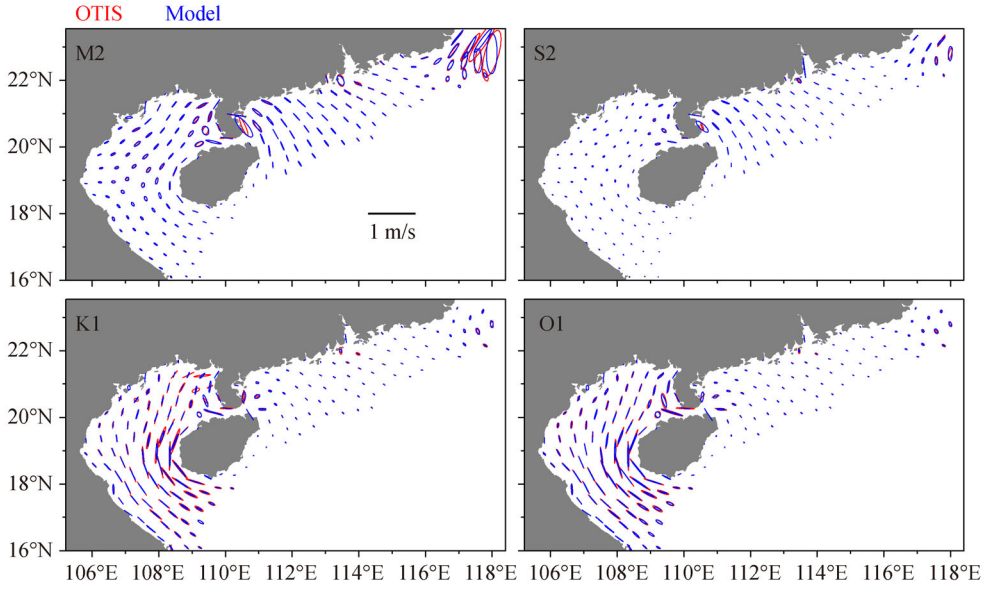

Fig. 4 Comparisons of tidal current ellipses for the four main tidal constituents between NSCS model and OTIS model.

suggested that semi-diurnal tidal currents dominated the NSCS shelf east of the Qiongzhou Strait while diurnal tidal currents prevailed the Beibu Gulf. The spatial distribution of tidal current ellipses was also in accordance with previous study of tidal currents in the SCS (Zu et al., 2008).

2.2.4 Daily mean sea level comparison

The model's fidelity in reproducing the daily mean sea level variations was examined by comparing the simulated long-time sea level time series at stations HK, SW, ZP, and BH with observations (Fig. 5). Direct comparisons indicate that the model is capable of capturing the low frequency sea level fluctuations throughout the course of simulation. The correlation coefficients between the two are 0.85 at HK, 0.77 at SW, 0.85 at ZP and 0.67 at BH (above 95% confidence level). The yearly cycle of the sea level elevations is also well reproduced by the model.

2.2.5 Seasonal mean currents comparison

Seasonal mean velocity vectors were computed by averaging the observed data over different seasons. We averaged the model results over the 18-year period at the mooring locations. Figure 6 shows the comparison between model-simulated and observed surface currents in the NSCS in different seasons. The root-mean-square errors (RMS) for the u and v component are also shown in the figure. The comparison indicates that the NSCS model generally captures the seasonal mean surface currents at the current stations. Both the observations and model results reveal southwestward currents in non-summer season, and northeastward currents in summer. The magnitude and direction differences may be attributed to the inaccurate surface forcing, topography, lateral open boundary condition and inaccurate parameterization used in the model. It should also be aware that the current observations are not repeated every year and the observational period lasted only for about one month, which further results in discrepancy for the seasonal mean current comparison. Generally, the comparison provides us the confidence that the NSCS model is able to resolve the seasonal mean circulation pattern over the NSCS shelf.

2.2.6 Temperature and salinity comparison

Figures 7 and 8 show the comparison between simulated and observed climatological monthly mean temperature and salinity over the NSCS shelf (depth < 200 m), respectively. Model-simulated bimonthly distributions of the climatological temperature and salinity at 20 m and 50 m over the NSCS shelf indicate that the NSCS model generally captures the seasonal evolution of the temperature and salinity. Both model results and observations show the northward intrusion of warm and saline water into the Beibu Gulf in winter and spring (January, March, and May in Figs. 7 and 8). The gradient of salinity in the northeast-southwest direction during winter and spring can also be noted both in the observations and simulation. In July, coastal upwelling induced by the predominant southwesterly monsoon became highly intensified and cold and saline water existed in the coastal region northeast of the Hainan Island and east of PRE (July in Figs. 7 and 8). In September, simulated temperature and salinity captured the cold and saline water mass in the southern region of the Beibu Gulf presented in the observations

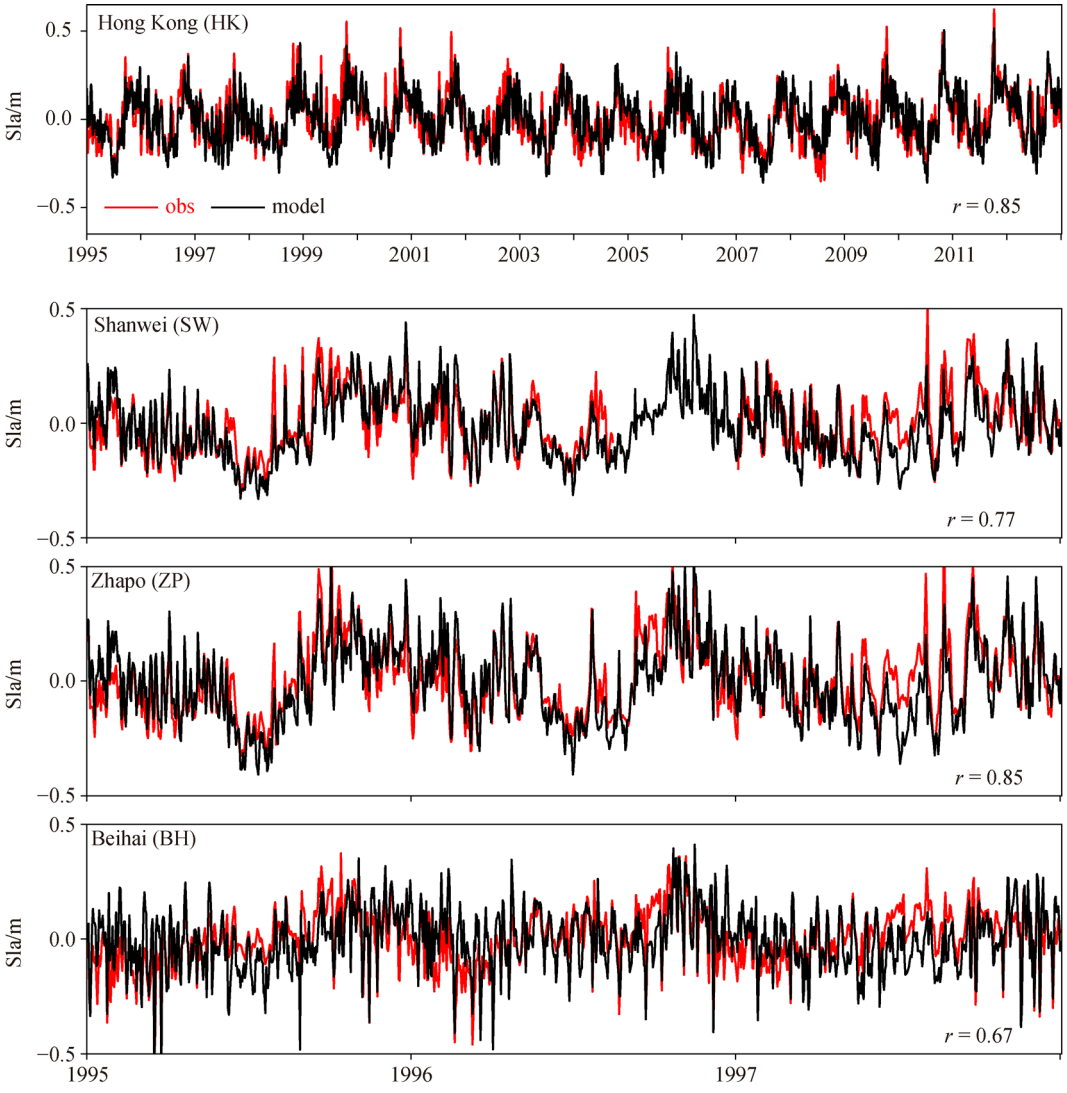

Fig. 5 Comparison of the modeled and observed daily sea level anomaly at station Hong Kong during 1995–2012, and at Shanwei, Zhapo, and Beihai during 1995–1997. The correlation coefficients between simulation and observations (r, above with 95% confidence level) are also indicated.

(September in Figs. 7 and 8). Additionally, both observed and simulated temperature in November indicate the southwestward alongshore movement of the cold water in coastal region east of the PRE. There are also mismatches in temperature and salinity between the simulation and observations. The surface forcing, freshwater discharge and uncertainties in the open boundary condition may lead to the difference between simulation and observations.

3 Seasonal mean circulation on the NSCS shelf

3.1 Mean circulation field

The seasonal variation SSH distribution is shown in Fig. 9. The climatology seasonal mean surface wind from NCEP/CFSR are also embedded in the figure. Northeasterly monsoon prevailed over the NSCS in winter (Fig. 9(a)), and the SSH increased southwestward to the Beibu Gulf due to Ekman transport. The highest SSH could reach more than 0.84 m. Similar SSH pattern could be observed in autumn due to similar wind fields (Fig. 9(d)). During summer, southwesterly monsoon dominates the NSCS and transports water northeastward, inducing low SSH over the NSCS (Fig. 9(c)). Low SSH cores formed northeast of Hainan and east of the PRE, where upwelling was strong under southwesterly monsoon (Hu and Wang, 2016). Climatological wind pattern during spring shows that southeasterly wind dominated the Beibu Gulf and the coastal region west of PRE while weak northeasterly wind prevailed in the east of the PRE (Fig. 9(b)). The northwestern coast of the Beibu Gulf and coastal region

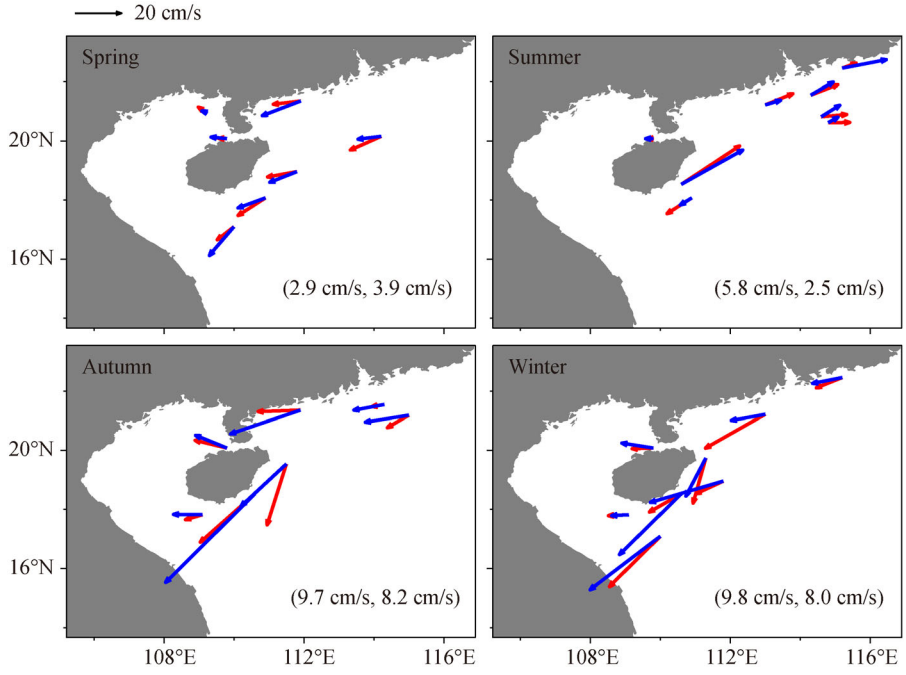

Fig. 6 Comparisons between simulated (blue) and observed (red; Zhang, 2014) seasonal mean surface currents. The root-mean-square errors (RMS) for the *u* and *v* component in different seasons are shown in parentheses.

west of the PRE were characterized by high SSH in spring. A high SSH band in the northeast of the Hainan Island extending northeastward along the 100 m isobath could also be noted.

Currents at 10 m and 50 m depths along with their respective standard deviations over the NSCS shelf are displayed in Fig. 10 and Fig. 11. The circulation at 10 m during winter is featured by southwestward currents in coastal NSCS (Fig. 10(a)). Under the northeasterly monsoon, southwestward down wind currents extended from southwest of Taiwan Strait to the east of the Qiongzhou Strait with 10–25 cm/s. The southwestward coastal currents diverted to the east of the Qiongzhou Strait. One branch flowed westward into the Beibu Gulf through the Qiongzhou Strait and the other turned southward along the southern coast of the Hainan Island with enhanced velocity. Weak northwestward currents existed on the NSCS outer shelf, transporting surface water in the continental slope region onto the shelf. The main dynamic feature in the sub-surface circulation of the Beibu Gulf in winter is the gulf-scale cyclonic gyre. The circulation pattern in the Beibu Gulf during winter agrees well with previous studies (Ding et al., 2013; Gao et al., 2013, 2017). The circulation pattern at 50 m depth in the NSCS during winter also features southwestward currents along the shelf (Fig. 11(a)). Strong currents existed east of PRE and make a cyclonic meandering mainly due to topography. Unlike the circulation pattern at 10 m depth, no northwestward onshore currents are observed at 50 m depth. The currents at 50 m depth generally flow southwestward across the shelf. The standard deviations of the velocity field maximized around the shelf break area, where southwestward propagating cyclonic and anti-cyclonic eddies and cross-shelf exchange often occur (Wang et al., 2008). Moreover, the boundary effects may also cause the large standard deviations.

The southwestward coastal currents at 10 m prevailed in the west segment of the NSCS (Fig. 10(b)). The southwestward coastal currents starting from the east of the PRE gradually strengthened westward and maximized to northeast of the Hainan Island. The northeastward current with magnitude of 5–10 cm/s flowed along the 50–100 m isobaths. This was in accordance with the high SSH band shown in Fig. 9(b). To the south of this northeastward current was the southwestward current along the shelf break. In the east segment of the NSCS shelf (east of the PRE), northeastward and eastward currents were dominant. The mean circulation pattern in the Beibu Gulf for spring is also featured by cyclonic circulation. A small enclosed cyclonic gyre was located in the northern head of the gulf and a stretched unclosed cyclonic gyre occupied the southern gulf, which was consistent with Gao et al. (2017). The mean circulation at 50 m depth over the NSCS shelf for spring is similar to that at 10 m depth with reduced velocity magnitude (Fig. 11(b)).

The simulated mean circulation pattern in summer is almost out of phase with that in winter (Fig. 10(c) and Fig. 11(c)). One of the most striking features is the strong northeastward currents over the NSCS shelf. From the surface circulation pattern (Fig.10(c)) we can see that the

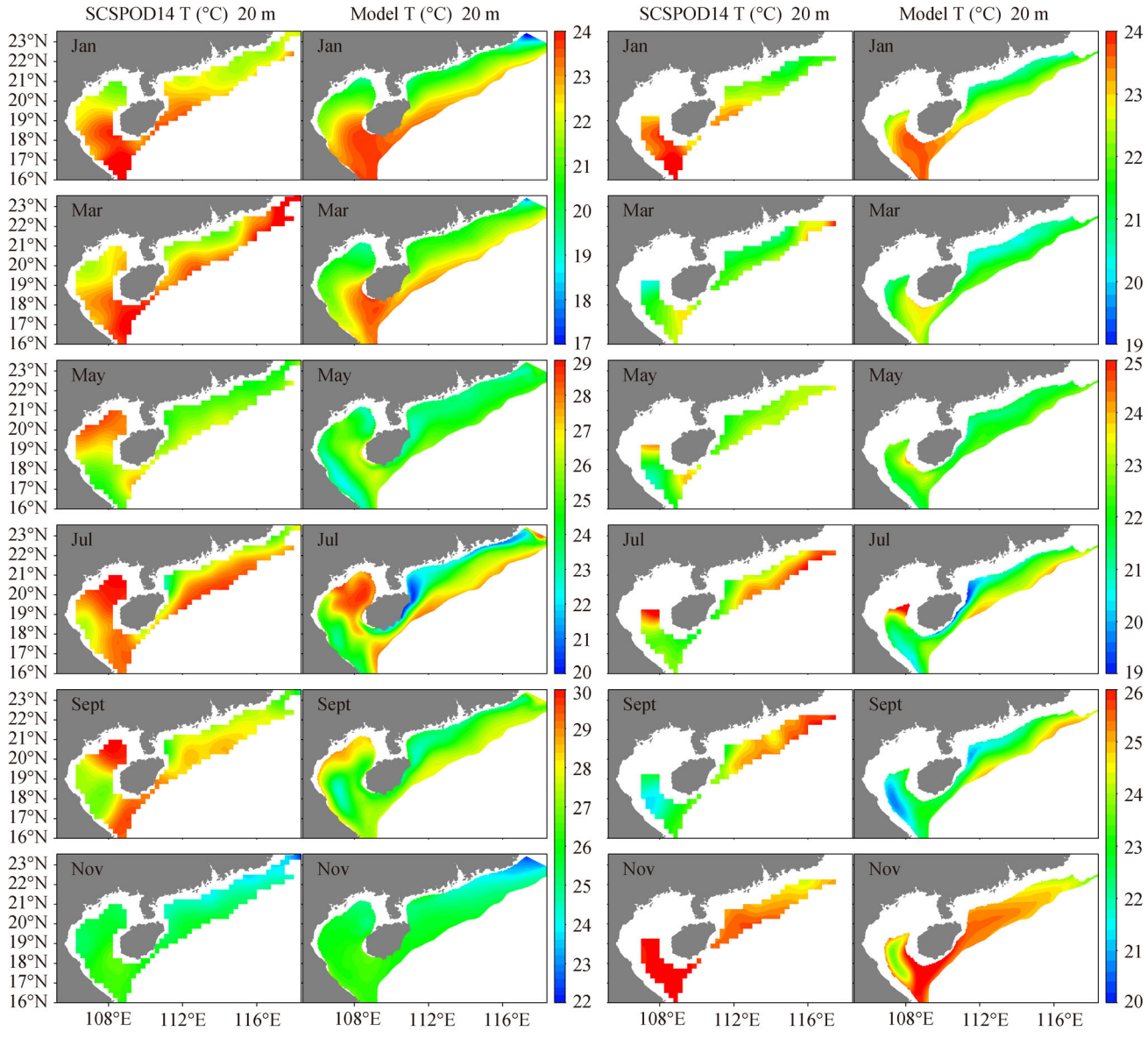

Fig. 7 Comparison of observed (SCSPOD14) and mode-simulated bimonthly temperature at 20 m and 50 m depth over the NSCS shelf (< 200 m depth).

strongest northeastward current exists southeast of the Hainan Island with magnitude exceeding 30 cm/s. The width of the northeastward current is large in the cross-shelf direction. It extended from the near shore region to the outer shelf in the NSCS. Part of the northeastward current veered cyclonically after passing the Hainan Island and meets the weak southwestward coastal current, giving rise to a small cyclonic eddy in the coastal region east of the Qiongzhou Strait. This cyclonic eddy east of the Qiongzhou strait during summer has been evidenced and discussed in previous studies (Bao et al., 2005; Song et al., 2012). The mean circulation was rather complex within the Beibu Gulf during summer. Anti-cyclonic circulation existed in the central gulf. In the southern gulf the southward alongshore current along the west coast of the gulf could be observed. The circulation at 50 m showed similar patterns to that at 10 m (Fig. 11(c)). However, to the south of the northeastward current, a southwestward current could be noted along the 200-m isobath.

In autumn, the mean circulation (Fig. 10(d) and Fig. 11 (d)) was similar to that in winter mentioned above, including the southwestward current along the NSCS shelf, bifurcation of the coastal current east of the Qiongzhou Strait, northwestward onshore current at surface layer, and the cyclonic gulf-scale gyre in the Beibu Gulf. We also noted that the intensity of the cyclonic gyre

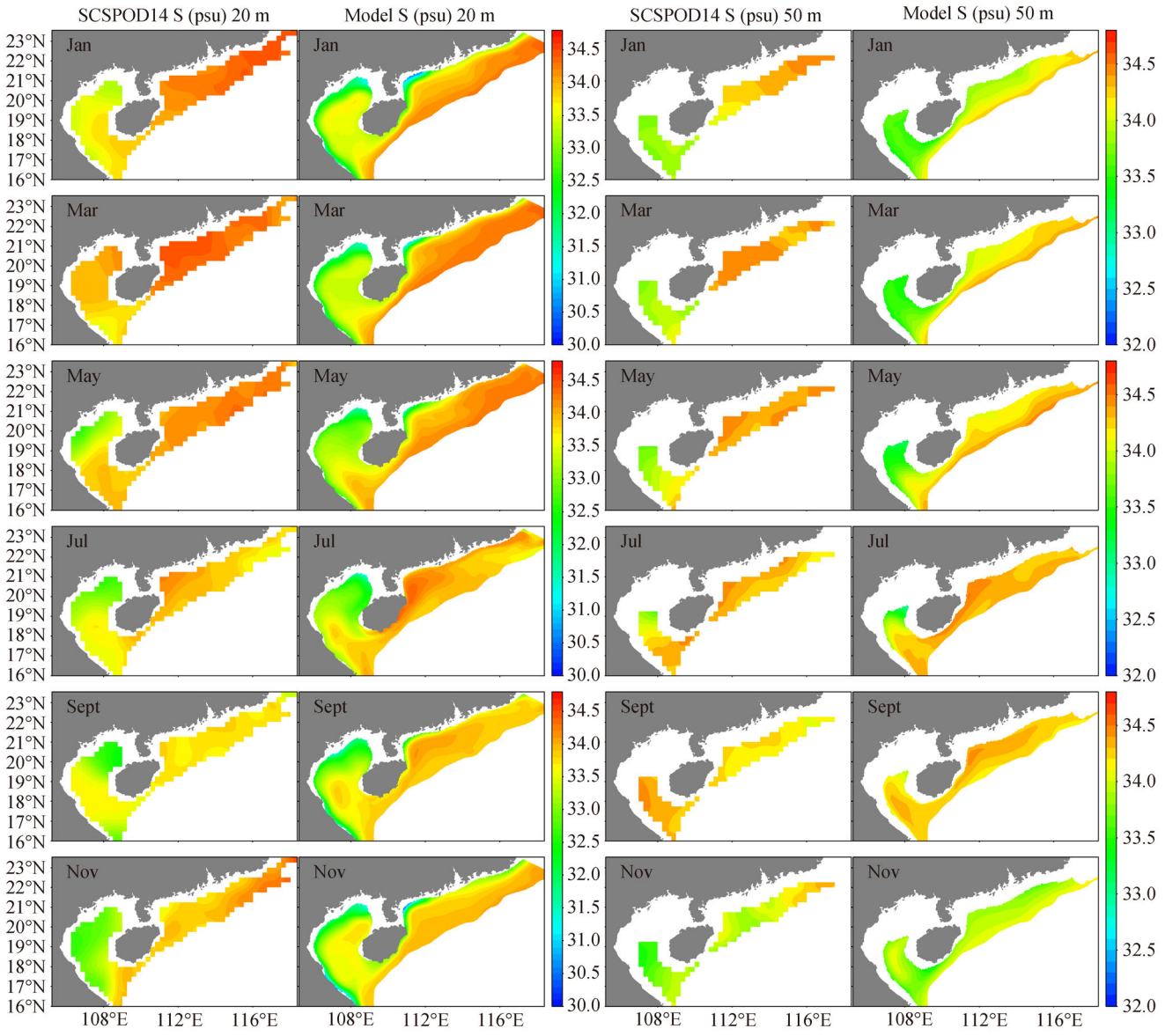

Fig. 8 Comparison of observed (SCSPOD14) and mode-simulated salinity at 20 m and 50 m depth over the NSCS shelf (< 200 m depth).

in the Beibu Gulf was stronger in autumn than that in winter, which is also evidenced by the review study of Gao et al. (2017).

3.2 Vertical structure of velocity and thermohaline distribution

Seasonal mean along-shelf and cross-shelf velocity, temperature, and salinity were examined along three cross-shelf transects in the NSCS (Figs. 12–15). The three cross-shelf transects locate offshore of station SW (Tr1), south of the PRE (Tr2), and offshore region of station ZP (Tr3; locations see Fig. 1). The model-simulated currents were projected to the normal and tangential directions for each transect to represent the along-shelf and cross-shelf velocities. Southwestward along-shelf and southeastward cross-shelf velocity were indicated by positive values in the figures.

3.2.1 Winter

In winter, similar temperature structures along Tr1, Tr2, and Tr3 can be observed (Fig. 12, column 1). The water was well mixed in coastal regions with water shallower than 50 m, mainly due to wind monsoon and strong tidal forcing. The salinity along the three transects during winter distributed homogeneously in a vertical direction (Fig. 12, column 2). However, cross-shelf salinity gradient can be

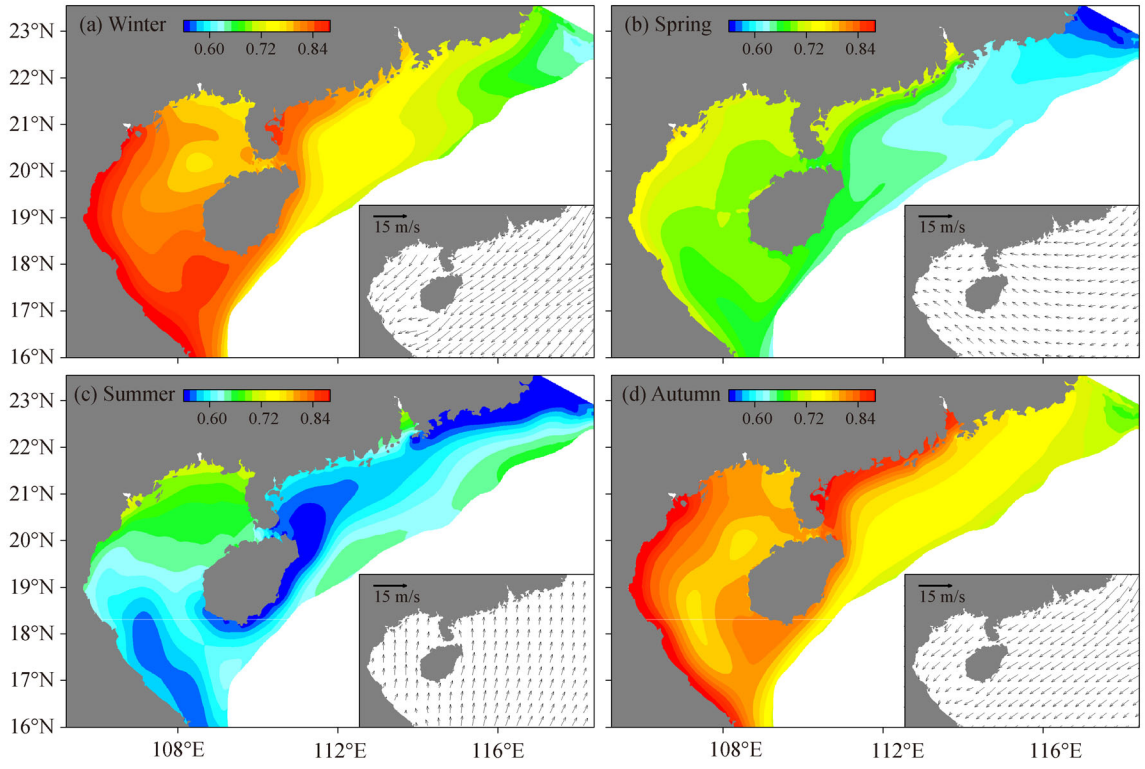

Fig. 9 Model-simulated seasonal mean sea surface height (color contour) and surface wind (vectors) from NCEP/CFSR averaged over the 18 years of 1995–2012. (a) Winter; (b) spring; (c) summer; (d) autumn.

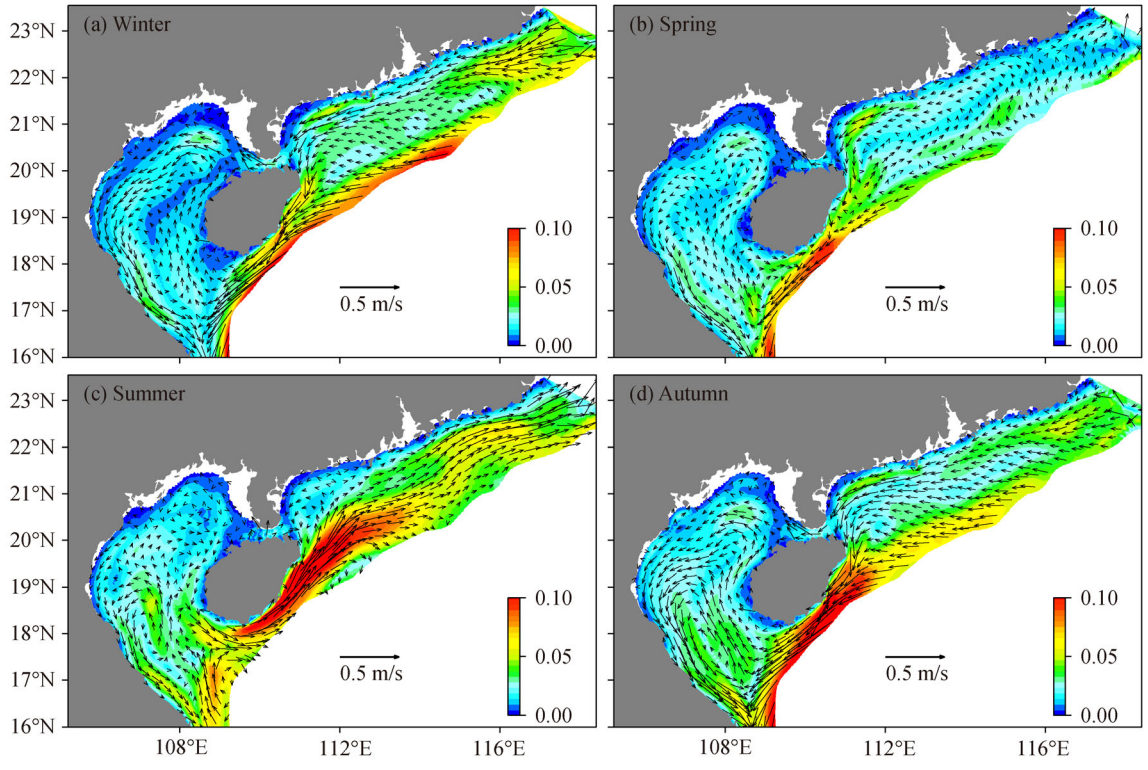

Fig. 10 Seasonal mean currents fields are shown in vectors and the standard deviations of the velocity are indicated by color contour at 10 m depth based on the 18-year model results. (a) Winter; (b) spring; (c) summer; (d) autumn.

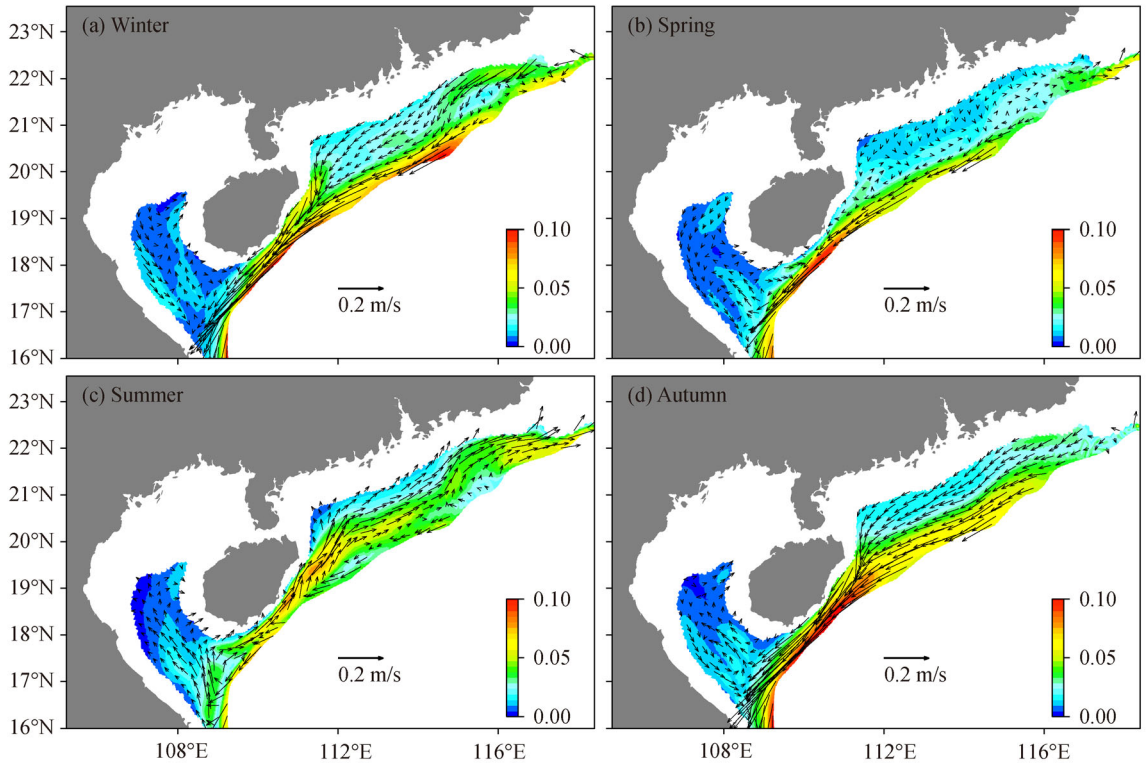

Fig. 11 Seasonal mean currents fields are shown in vectors and the standard deviations of the velocity are indicated by color contour at 50 m depth based on the 18-year model results. (a) Winter; (b) spring; (c) summer; (d) autumn.

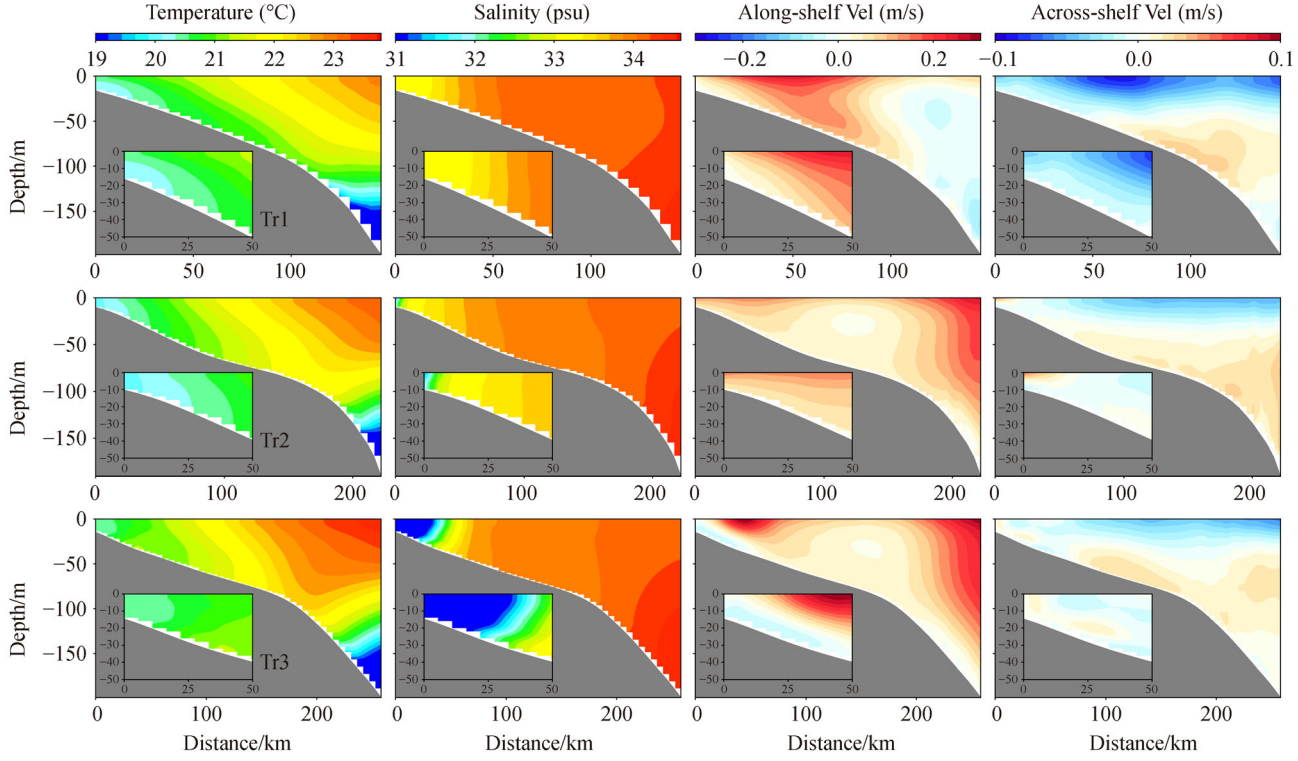

Fig. 12 Mean cross-shelf transects of temperature, salinity, along-shelf and cross-shelf velocity in winter. The upper panel for Tr1, middle panel for Tr2 and lower panel for Tr3. For along-shelf and cross-shelf velocity, positive values indicate southwestward and offshore and negative values indicate northeastward and onshore. The structures of temperature, salinity, along-shelf and cross-shelf velocity within the coastal region shallower than 50 m are enlarged and embedded in the figure.

noted along all transects. The shelf water was fresher near the coastal region than offshore. The distinctive cross-shelf salinity gradient could be observed along transect Tr2. Low-salinity water from the PRE was trapped near the coastal region west of Guangdong under the winter monsoon, which induced the prominent cross-shelf salinity gradient along transect Tr3.

Distributions of along-shelf velocity along three transects indicated the consistent southwestward current over the NSCS shelf (Fig. 12, column 3). The southwestward current intensified along the NSCS shelf from Tr1 down to Tr3. Northeastward current was detected in the offshore region of Tr1 and bottom layer of Tr3 with less than 10 cm/s. The southwestward current was limited in the regions with depth shallower than 100 m along transect Tr1. Along transect Tr2 and Tr3, the southwestward current extended to the offshore region more than 200 km away from the coast. Strong southwestward currents reaching 20 cm/s distributed nearshore and over the shelf break along transects Tr2 and Tr3, and the southwestward current over the outer shelf area with depth 50–100 m was weak with magnitude of 5–10 cm/s.

Cross-shelf velocities along three transects illustrated onshore current in the upper layer (depth < 50 m) and offshore current in the lower layer. The magnitude of the cross-shelf current (< 10 cm/s) was weaker than the along-shelf current.

3.2.2 Spring

In spring similar temperature structure along the three transects could be observed. The vertical distributions of temperature and salinity along the transects showed that the water was more stratified compared to that during winter (Fig. 13, column 1). The temperature gradient in the cross-shelf direction was smaller compared to that in winter. Over the inner shelf ($h < 50$ m), the temperature difference between surface and bottom layer ranged from 1°C to 4°C.

Salinity distributions along the transects showed that freshwater moved seaward in the upper layer (Fig. 13, column 2). The vertical salinity gradient in the coastal region was larger than that in winter. As the southwestward alongshore current prevailed west of Guangdong in spring (Fig. 10(b)), low-salinity water was transported westward along the coast, and the salinity front along the transect Tr3 dispersed more offshore than that along the transect Tr2.

The northeastward along-shelf velocity with magnitude of 5–10 cm/s dominated transect Tr1 east of the PRE, indicating the northeastward current prevailed over the east segment of the NSCS shelf (Fig. 13, column 3). Along transects Tr2 and Tr3, the southwestward along shelf current prevailed over the coastal area with depth shallower than 50 m and also offshore regions with depth deeper than 100 m. A predominant feature over the west segment of the NSCS shelf (Tr2 and Tr3) was the

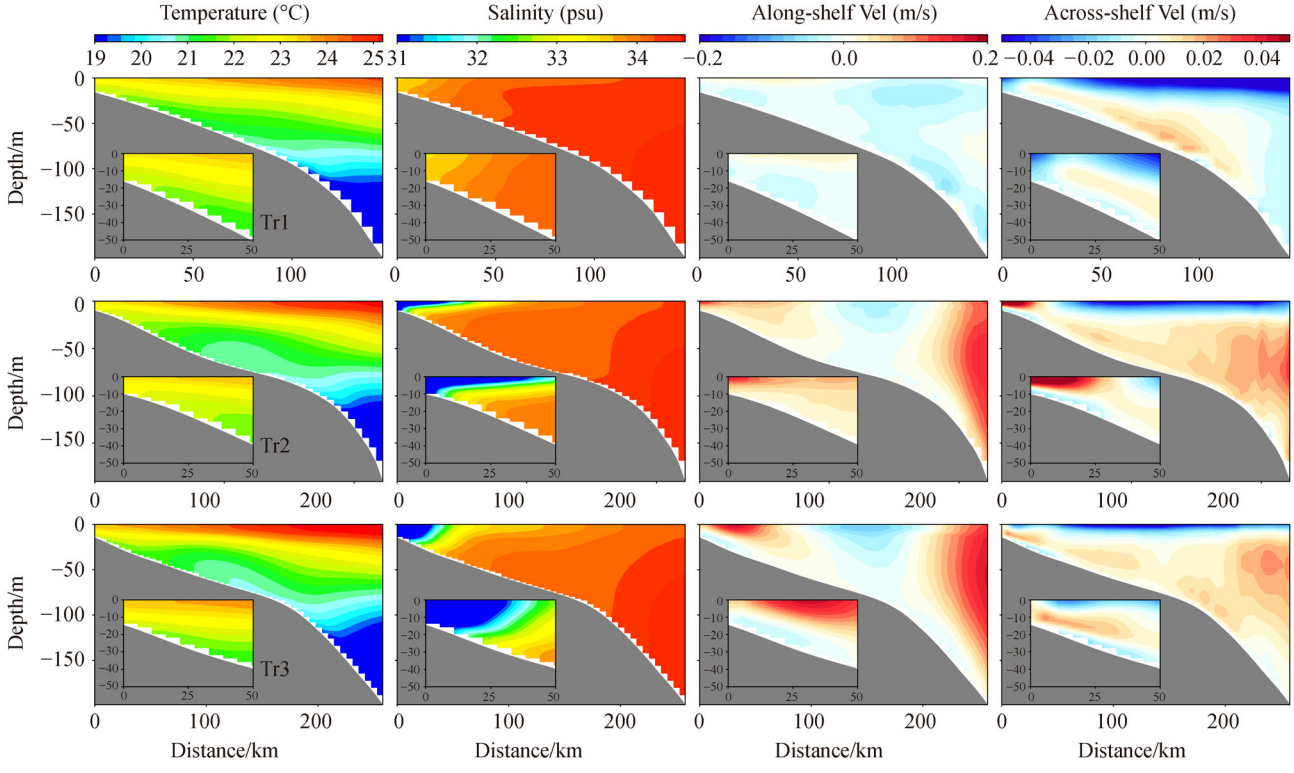

Fig. 13 Same as Fig. 12, but for spring.

weak northeastward current along the 50–100 m isobaths. This current was different from the SCSWC that was considered to be flowing along 100–200 m isobaths. The southwestward current peaked at ~50 km offshore.

The cross-shelf velocity in spring (Fig. 13, column 4) was similar to that in winter. Onshore flow in the upper layer and offshore flow in the lower layer was prevalent along transect Tr1, Tr2, and Tr3. However, the onshore flow was rather weak with velocity less than 5 cm/s and was limited within the upper layer (depth < 20 m).

3.2.3 Summer

Temperature and salinity structures in summer indicated substantial water stratification through the entire shelf even in coastal areas (Fig. 14, column 1 and 2). This is due to increased heat flux and decreased mixing process induced by winds. The temperature difference in the vertical direction went up compared to that in spring mainly due to enhanced surface heating in summer. SST exceeded 29°C along all the transects. The temperature difference between the surface and bottom layers reached 4°C in coastal region and more than 9°C in offshore region. Intensified upwelling over the NSCS shelf can be found in the temperature structure along the three transects. Bottom cold water was uplifted onshore and in the coastal region under the upwelling favorable monsoon wind during summer.

Salinity along the transects show that freshwater spread offshore under southwesterly monsoon, which was especially conspicuous along transects Tr2 and Tr3 (Fig. 14, column 2). This could be attributed to the river plume south of the Pearl River extending offshore to the mid-shelf (Tr2) under southwesterly wind. The salinity gradient decreased offshore along all the four transects. The tilted salinity front was found along transect Tr3, where the upper layer of the front moved offshore while the lower layer of the front moved onshore. It can also be noted that the salinity gradient in the vertical direction during summer was larger than that during winter and spring, which further intensified the stratification of the water column.

Along-shelf velocity indicates that northeastward current was prevalent over the NSCS shelf (Fig. 14, column 3). Southwestward coastal current is limited in near shore area with depth shallower than 10 m. Moreover, southwestward current is also evidenced in the shelf break area. Strong northeastward current occurs in the upper layer and gradually decreased with depth.

Mean cross-shelf velocity panels (Fig. 14, column 4) show that offshore flow is most obvious along transect Tr1 at the east segment of the NSCS shelf. The offshore flow occupies most of the water column along Tr1 while it only

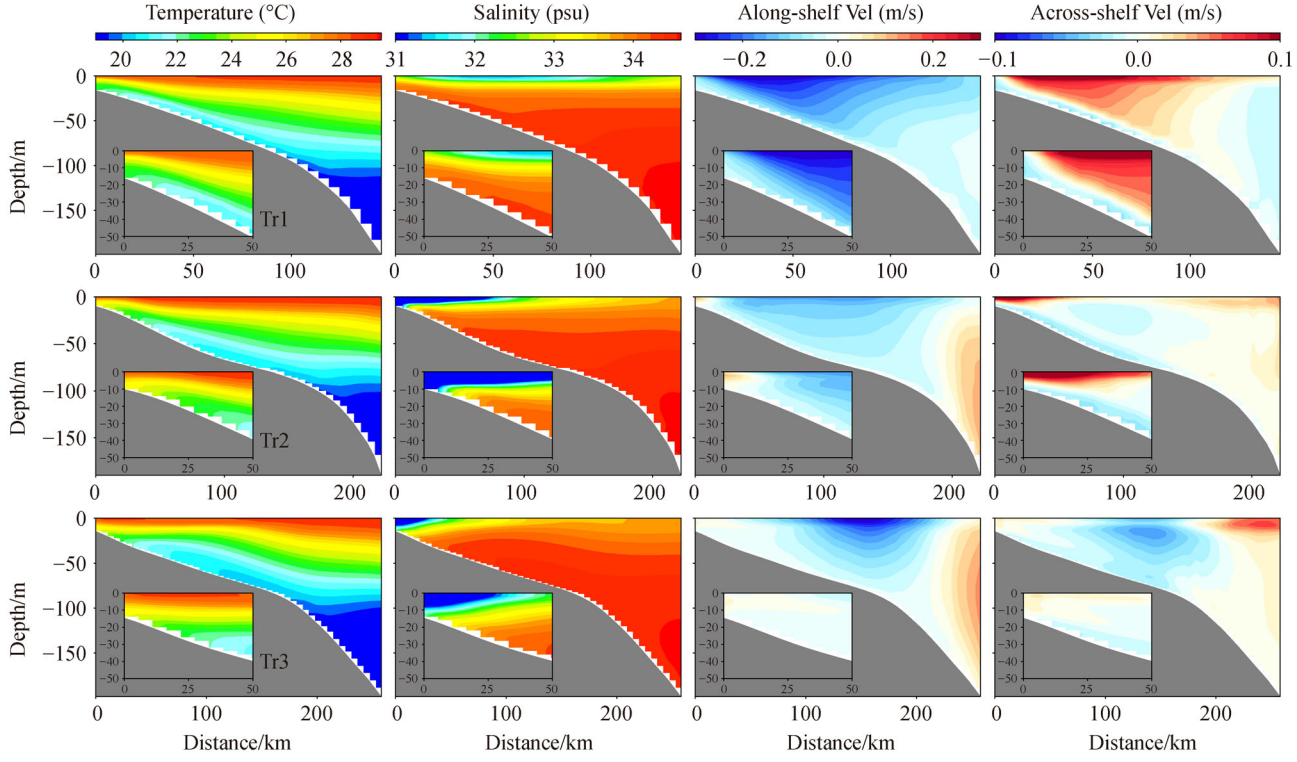

Fig. 14 Same as Fig. 12, but for summer.

occurs in the surface layer in the other three transects. Onshore flow can be observed in the bottom (Tr1) or the lower layer (Tr2, Tr3) over the shelf.

3.2.4 Autumn

Mean temperature transects during autumn (Fig. 15, column 1) exhibit similar pattern to spring and summer. The thermal stratification is still remarkable over the NSCS shelf. Increasing temperature from north to south can also be observed from the cross-shelf temperature structure. Mean salinity structures along the cross shelf transects in autumn are similar to that in spring. Low-salinity water is mainly confined along the coastal region with the recovery of the northeasterly wind in autumn.

Along-shelf velocity (Fig. 15, column 3) and cross-shelf velocity (Fig. 15, column 4) in autumn show very similar pattern to that in winter. Southwestward currents are evidenced along the entire shelf. Cross-shelf velocity is characterized by onshore flow in the upper layer and offshore flow in the lower layer, which also shows similar pattern to that in winter.

It is important to note that the winter mean circulation pattern over the NSCS shelf does not support the existence of the permanent counter-wind South China Sea Warm Current (SCSWC) flowing northeastward along the 100–200 m isobaths. It is interesting that previous observational study based on long-term direct current measurements did not observed the permanent SCSWC during wintertime (Li et al., 2014).

4 Seasonal along- and cross-shelf transport

Quantifying the water transport in along-shelf and cross-shelf directions and their seasonal variability in the NSCS is essential for investigating the heat flux, freshwater, and nutrients transport, which are crucial to the coastal circulation and ecosystem over the NSCS shelf. In addition, examining the cross-shelf transport is vital to understand the material exchange between the shelf and open oceans. In this section we aim to estimate the seasonal mean along- and cross-shelf transport in the NSCS based on the model hindcast results. The 200 m isobath is defined to be the boundary between shelf sea and slope area (black line in Fig. 1). Six cross-shelf transects from south of Taiwan Strait to southeast of the Hainan Island were selected (Fig. 16 red lines). These cross-shelf transects start from the coastline and extend offshore until the 200 m isobath. The currents were projected to the normal and tangential directions for each transect. The velocity in the normal direction was used to calculate the volume transport across each transect.

The seasonal along-shelf and cross-shelf transport with their standard deviations (SDs) are calculated based on the 18-year model simulation (Fig. 16). In winter (Fig. 16(a)),

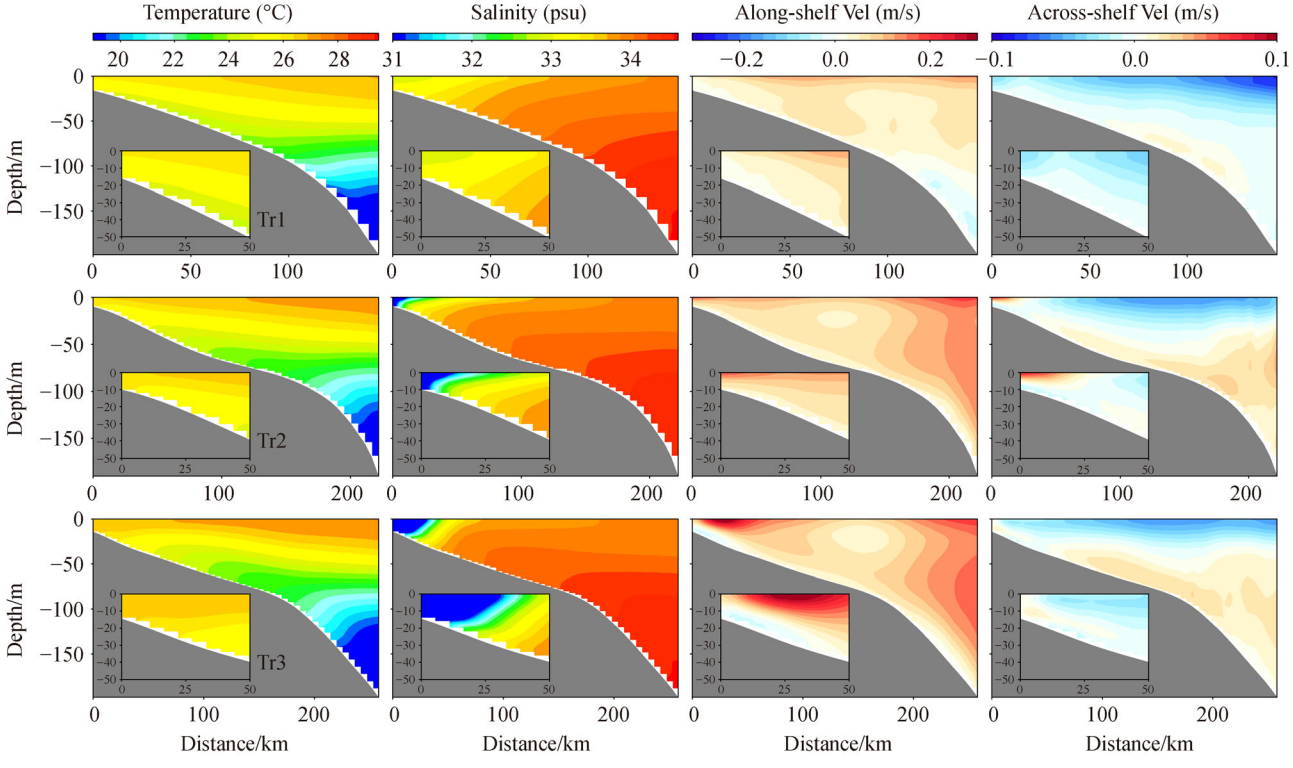

Fig. 15 Same as Fig. 12, but for autumn.

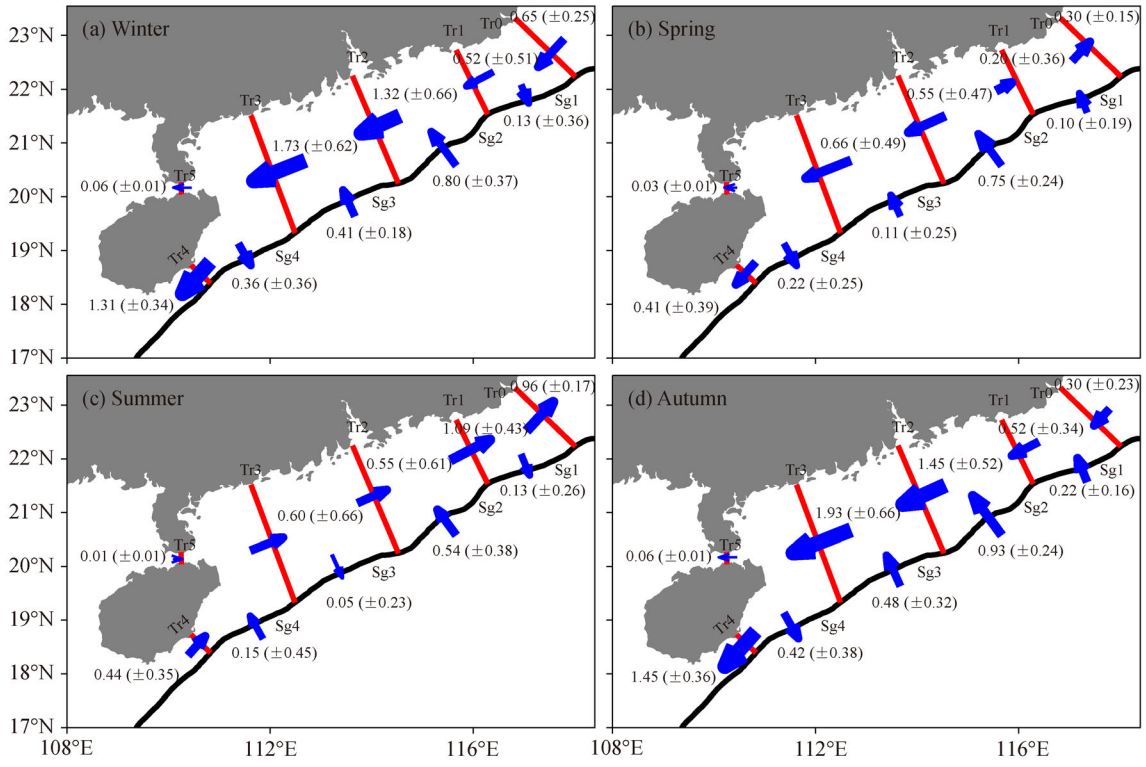

Fig. 16 A schematic view for the model-calculated along-shelf and cross-shelf transport over the NSCS shelf during four seasons. The mean values of transport (in Sv) and their standard deviations (in parentheses) are shown in the figure. (a) Winter; (b) spring; (c) summer; (d) autumn.

the mean along-shelf transport featured a gradual downstream increment over the NSCS shelf, increasing from 0.65 Sv along the easternmost transect (Tr0) to 1.73 Sv along the transect west of the PRE (Tr3). However, there was a reduction of transport from 1.73 Sv along the transect west of the PRE (Tr3) to 1.31 Sv along the transect southeast the Hainan Island (Tr4). The westward transport across the Qiongzhou Strait is estimated to be 0.06 Sv, which is comparable to the transport value of 0.02–0.048 Sv from Yan et al. (2008) and 0.055 Sv from Chen et al. (2007b) based on observations. Based on observed currents during 2006–2007, Fang et al. (2015) estimated the southwestward along-shelf transport crossing a transect near Tr2 to be 2.0 Sv in winter. Our estimation through Tr2 is 1.32 Sv with standard deviation of 0.66 Sv, which matches the observed value. In the western segment of the NSCS shelf, the SDs along transect Tr0 and Tr1 are of the same order of magnitude to the mean transport. The cross-shelf sea level gradient induced by the Kuroshio intrusion southwest of Taiwan Island may be responsible for the along-shelf flow reversals during winter (Yang et al., 2002; Xue et al., 2004; Yang, 2007). The along-shelf transport is balanced by cross-shelf transport. Thus, the winter mean cross-shelf transport is shoreward across segments of the 200 m isobaths (Sg2 and Sg3) with onshore transport value reaching 1.21 Sv (0.80 Sv for Sg2, 0.41 Sv for Sg3). The offshore transport is about 0.49 Sv, which mainly occur along the easternmost segment (Sg1, 0.13 Sv) and western segment (Sg4, 0.36 Sv) of the 200 m isobath.

In spring (Fig. 16(b)), the mean along-shelf transport is northeastward in the eastern segment of the NSCS shelf along Tr0 and Tr1, while is southwestward in the western segment along Tr2, Tr3, and Tr4. The southwestward transport ranges from 0.41 Sv across Tr4 to 0.66 Sv across Tr3. The transport through Tr2 in our model is 0.55 Sv with standard deviation of 0.47 Sv, which is smaller compared with the observed value of 2.1 Sv (Fang et al., 2015). This may be due to interannual variability of the transport. The westward transport across the Qiongzhou Strait is about 0.03 Sv estimated in our model results. Based on observed current data, Zhu et al. (2014) estimated the westward transport across the Qiongzhou Strait to be 0.065 Sv, which is of the same order to the transport value calculated in our model. The SDs are comparable to the values of the along-shelf mean transport values across all the transects. Spring is a transitional period of monsoons and local winds influence the shelf circulation in the NSCS. Therefore, flow reversals usually occur during spring and induce large SDs for the along-shelf transport. In the cross-shelf direction, the mean cross-shelf transport pattern is similar to that in winter, when onshore water movement mainly occurs across the 200 m isobath south of the PRE (Sg2 and Sg3). The onshore transport across the 200 m is about 0.96 Sv (0.10 Sv for Sg1, 0.75 Sv for Sg2, and 0.11 Sv for Sg3),

and the offshore transport is estimated to be 0.22 Sv across Sg4.

The mean along-shelf transport in summer (Fig. 16(c)) is opposite to that in winter. Along-shelf transport over the NSCS shelf range from 0.44 Sv across transect southeast of Hainan (Tr4) to 1.09 Sv across transect east of the PRE (Tr1). SDs of the western segment of the NSCS shelf (Tr2, Tr3, and Tr4) are comparable to the mean values of along-shelf transport, suggesting the highly fluctuated northeastward along-shelf current in the western NSCS shelf during summer. Such variability of along-shelf current in summer may be related to local winds (southwesterly or southeasterly wind), spreading of the Pearl River plume, and frequent typhoons. It should be noted that Fang et al. (2015) calculated the transport through a section very near Tr2 to be northeastward with mean value of 1.4 Sv during summer, which is larger than our estimation (0.55 Sv with standard deviation 0.61 Sv). The disagreement may be due to the interannual variation of the shelf circulation. The model-estimated transport across the Qiongzhou Strait in summer is about 0.01 Sv eastward. The current structure in the Qiongzhou Strait during summer is still under debate, and transport in the strait remains controversial. Based on limited and short-term observations, Shi et al. (2002) calculated the summer transport in the Qiongzhou Strait to be 0.1–0.2 Sv westward. However, Chen (2013) proposed that the transport in the strait during summer ranged from 0.05 Sv westward to 0.05 Sv eastward based on a numerical model. Cross-shelf transport values feature small means and large SDs except across transect Sg2 southeast of the PRE, where the SDs are of the same order with the mean cross-shelf transport value. Similar to winter and spring, relatively large onshore transport of 0.54 Sv in summer also occurs across the 200 m segment southeast of the PRE (Sg2).

The mean along-shelf and cross-shelf transport in autumn (Fig. 16(d)) show similar pattern to that in winter. The gradual downstream increment of the mean along-shelf transport can be noted, increasing from 0.30 Sv across transect Tr0 south of the Taiwan Strait to 1.93 Sv across transect Tr3 west of the PRE. The mean along-shelf transport values in autumn are larger than that in winter across the transects over the west segment of the NSCS shelf (Tr2, Tr3, and Tr4). Our estimation of transport through Tr2 (1.45 Sv) is larger than the observed value (0.9 Sv) by Fang et al. (2015) It should also be noted that the mean cross-shelf transport values in autumn are larger than the other three seasons. A total of 1.63 Sv of the slope water is transported onto the shelf sea across the 200 m isobaths (0.22 Sv for Sg1, 0.93 Sv for Sg2, and 0.48 Sv for Sg3). Offshore transport of 0.42 Sv mainly occurs across Sg4.

It is worth noting that the cross-shelf transport across the segment of 200 m isobath south of the PRE (Sg2 and Sg3) is shoreward in all seasons except in summer at Sg3 with small seaward mean and large SDs. This suggests that these areas are imported sites for shelf water import. Offshore cross-shelf transport across 200 m isobath mainly occurs at the region southeast of the Hainan Island (Sg4). It should also be noted that in the cross-shelf direction the SDs are of the same order of magnitude to the mean cross-shelf transport values during each season, and even larger than the mean values in summer. This suggests that the interactions between shelf region and slope sea in the NSCS are highly variable. The water exchange between shelf and deep sea may be influenced by local variable wind and also mesoscale eddies that propagate southwestward along the continental slope in the NSCS (Wang et al., 2003; Wang et al., 2008; Fang et al., 2015; Zhang et al., 2016).

More extensive model-data comparisons may be required in future research, as the observed data used in the current study is relatively inadequate. The clear mismatch in the currents, temperature, and salinity between the NSCS model and observations can be noted, which will be further reduced by using higher model resolution and method of assimilation of observed profiles of temperature and salinity from *in-situ* CTDs and also Argo floats.

5 Summary

To study the seasonal mean circulation over the NSCS shelf, a regional ocean model focusing on the NSCS based on FVCOM was established. Model-data comparisons show that the NSCS model generally resolves the seasonal variations of the NSCS shelf circulation.

The 18-year model hindcast results from 1995–2012 were utilized to examine the characteristics of the seasonal mean circulation and the three-dimensional structures over the NSCS shelf. The mean circulation over the NSCS features prominent seasonal variability corresponding to the monsoon. Southwestward currents dominate the NSCS shelf in winter and autumn while northeastward currents prevail in summer. The circulation pattern in spring is more complex than the other seasons. The most obvious feature of the circulation pattern in the Beibu Gulf is the persistence of a gulf-scale cyclonic gyre, although this cyclonic gyre is significantly weakened and mainly confined in the southern gulf during summer. Cross-shelf velocity during winter (summer) is characterized by onshore (offshore) flow in the upper layer and offshore (onshore) in the lower layer. However, our model results indicate a northeastward current flowing along 50–100 m isobaths in spring. This current should be focused on in future studies based on both observations and numerical models.

The along-shelf and cross-shelf transport in different seasons were also quantified.

The along-shelf transport increases southwestward over the NSCS shelf in winter and autumn. The cross-shelf

transport features high variability, with standard deviations comparable or even larger than the mean values. Maximum cross-shelf onshore transport is noted around the shelf break segment south of the PRE, suggesting this area is the major site for onshore intrusion of slope water.

Acknowledgements This work was jointly supported by the National Natural Science Foundation of China (Grant Nos. 41606005, 41676004, 41506027, and 41476047), National Program on Global Change and Air-Sea Interaction (No. GASI–GEOGE 03), National Fund Committee-Shandong joint fund (No. U1706215), the Fundamental Research Funds for the Central Universities (201713023), the Project of State Key Laboratory of Satellite Ocean Environment Dynamics, Second Institute of Oceanography (No. SOEDZZ1805) and the National Key Research and Development Plan (2016YFC1401406 and 2016YFA0600900). All the model simulations are performed in the Ocean Data and Simulation Center of Physical Oceanography Laboratory, Ocean University of China. We thank University of Hawaii Sea Level Center, National Center for Environmental Prediction (NCEP), Hybrid Coordinate Ocean Model, and OSU Tidal Data Inversion for providing valuable data. We also thank the two anonymous reviewers for careful review and constructive comments.

References

Álvarez-Salgado X A, Gago J, Míguez B M, Pérez F F (2001). Net ecosystem production of dissolved organic carbon in a coastal upwelling system: the Ria de Vigo, Iberian margin of the North Atlantic. Limnol Oceanogr, 46(1): 135–146

Bao X, Hou Y, Chen C, Chen F, Shi M (2005). Analysis of characteristics and mechanism of current system on the west coast of Guangdong of China in summer. Acta Oceanol Sin, 24: 1–9

Bleck R (2002). An oceanic general circulation model framed in hybrid isopycnic-Cartesian coordinates. Ocean Model, 4(1): 55–88

Cai S, Su J, Gan Z, Liu Q (2002). The numerical study of the South China Sea upper circulation characteristics and its dynamic mechanism, in winter. Cont Shelf Res, 22(15): 2247–2264

Chassignet E P, Hurlburt H E, Smedstad O M, Halliwell G R, Hogan P J, Wallcraft A J, Baraille R, Bleck R (2007). The HYCOM (hybrid coordinate ocean model) data assimilative system. J Mar Syst, 65(1–4): 60–83

Chen B, Yan J, Wang D, Shi M (2007b). The transport volume of water through the Qiongzhou Strait in the winter season. Period Ocean Univ China, 37: 357–364 (in Chinese)

Chen C, Huang H, Beardsley R, Liu H, Xu Q, Cowles G (2007a). A finite-volume numerical approach for coastal ocean circulation studies: comparisons with finite difference models. J Geophys Res, 112(C3): C03018

Chen C, Lai Z, Beardsley R, Xu Q, Lin H, Viet N T (2012). Current separation and upwelling over the southeast shelf of Vietnam in the South China Sea. J Geophys Res, 117(C3): C03033

Chen C, Liu H, Beardsley R (2003). An unstructured, finite-volume, three-dimensional, primitive equation ocean model: application to coastal ocean and estuaries. J Atmos Ocean Technol, 20(1): 159–186

Chen C, Wang S, Wang B, Pai S (2001). Nutrients budgets for the South China Sea basin. Mar Chem, 75(4): 281–300

Chen Z (2013). Numerical Simulation on Seasonal Variation of Ocean Circulation and Its Dynamic Mechanism in the Beibu Gulf. Dissertation for Ph.D Degree. Qingdao: Ocean University of China (in Chinese)

Chen Z, Gong W, Cai H, Chen Y, Zhang H (2017). Dispersal of the Pearl River plume over continental shelf in summer. Estuar, Coast Shelf Res, 194: 252–262

Chen Z, Pan J, Jiang Y (2016). Role of pulsed winds on detachment of low salinity water from the Pearl River Plume: upwelling and mixing processes. J Geophys Res, 121, doi: 10.1002/2015JC011337

Chern C S, Jan S, Wang J (2010). Numerical study of mean flow patterns in the South China Sea and the Luzon Strait. Ocean Dyn, 60(5): 1047–1059

Chiang T L, Wu C R, Chao S Y (2008). Physical and geographical origins of the South China Sea warm current. J Geophys Res, 113 (C8): C08028

Ding Y, Bao X, Yao Z, Zhang C, Wan K, Bao M, Li R, Shi M (2017). A modeling study of the characteristics and mechanism of the westward coastal current during summer in the northwestern South China Sea. Ocean Science Journal, 52(1): 11–30

Ding Y, Chen C, Beardsley R C, Bao X, Shi M, Zhang Y, Lai Z, Li R, Lin H, Viet N T (2013). Observational and model studies of the circulation in the Gulf of Tonkin, South China Sea. J Geophys Res Oceans, 118(12): 6495–6510

Egbert G, Erofeeva S (2002). Efficient inverse modeling of barotropic ocean tides. J Atmos Ocean Technol, 19(2): 183–204

Fang G, Fang W, Fang Y, Wang K (1998). A survey of studies on the South China Sea upper ocean circulation. Acta Oceanogr Taiwanica, 37(1): 1–16

Fang W D, Guo P, Liu C J, Fang G H, Li S J (2015). Observed sub-inertial current variability and volume transport over the continental shelf in the northern South China Sea. Estuar Coast Shelf Sci, 157: 19–31

Gan J P, Wang J J, Liang L L, Li L, Guo X G (2015). A modeling study of the formation, maintenance, and relaxation of upwelling circulation on the Northeastern South China Sea shelf. Deep Sea Res Part II Top Stud Oceanogr, 117: 41–52

Gan J, Cheung A, Guo X, Li L (2009a). Intensified upwelling over a widened shelf in the northeastern South China Sea. J Geophys Res, 114(C9): C09019

Gan J, Li L, Wang D, Guo X (2009b). Interaction of a river plume with coastal upwelling in the northeastern South China Sea. Cont Shelf Res, 29(4): 728–740

Gan J, Lu Z, Dai M, Cheung A Y Y, Liu H, Harrison P (2010). Biological response to intensified upwelling and to a river plume in the northeastern South China Sea: a modeling study. J Geophys Res, 115(C9): C09001

Gan J, San Ho H S, Liang L (2013). Dynamics of intensified downwelling circulation over a widened shelf. J Phys Oceanogr, 43 (1): 80–94

Gao J, Wu G, Ya H (2017). Review of the circulation in the Beibu Gulf, South China Sea. Cont Shelf Res, 138: 106–119

Gao J, Xue H, Chai F, Shi M (2013). Modeling the circulation in the Gulf of Tonkin, South China Sea. Ocean Dyn, 63(8): 979–993

Guan B, Chen S (1964). The Current Systems in the Near-Sea Area of China Seas. Technical Report, Institute of Oceanology, Qingdao, China, 1–85 (in Chinese)

Guan B, Fang G (2006). Winter counter-wind currents off the

southeastern China coast: a review. J Oceanogr, 62(1): 1–24

Han A, Dai M, Kao S, Gan J, Li Q, Wang L, Zhai W, Wang L (2012). Nutrient dynamics and biological consumption in a large continental shelf system under the influence of both a river plume and coastal upwelling. Limnol Oceanogr, 57(2): 486–502

Hill J K, Wheeler P A (2002). Organic carbon and nitrogen in the northern California current system: comparison of offshore, river plume, and coastally upwelled water. Prog Oceanogr, 53(2–4): 369–387

Hu J Y, Kawamura H, Hong H, Qi Y (2000). A review on the currents in the South China Sea: seasonal circulation, South China Sea warm current and Kuroshio intrusion. J Oceanogr, 56(6): 607–624

Hu J, Wang X H (2016). Progress on upwelling studies in the China seas. Rev Geophys, 54(3): 653–673

Ji X, Sheng J, Zheng J, Zhang W (2015). Numerical study of seasonal circulation and variability over the inner shelf of the northern South China Sea. Ocean Dyn, 65(8): 1103–1120

Lai Z, Ma R, Gao G, Chen C, Beardsley R C (2015). Impact of multichannel river network on the plume dynamics in the Pearl River estuary. J Geophys Res Oceans, 120(8): 5766–5789

Li Q P, Wang Y, Dong Y, Gan J (2015). Modeling long-term change of planktonic ecosystems in the northern South China Sea and the upstream Kuroshio Current. J Geophys Res Oceans, 120(6): 3913–3936

Li R, Chen C, Xia H, Beardsley R C, Shi M, Lai Z, Lin H, Feng Y, Liu C, Xu Q, Ding Y, Zhang Y (2014). Observed wintertime tidal and subtidal currents over the continental shelf in the northern South China Sea. J Geophys Res Oceans, 119(8): 5289–5310

Lin P, Cheng P, Gan J, Hu J (2016). Dynamics of wind-driven upwelling off the northeastern coast of Hainan Island. J Geophys Res Oceans, 121(2): 1160–1173

Liu X, Su J (1993). A numerical model of winter circulation in shelf seas adjacent to China. Proceedings of the Symposium on the Physical and Chemical Oceanography of the China Seas. Beijing: China Ocean Press, 288–298

Liu Z, Gan J (2017). Three-dimensional pathways of water masses in the South China Sea: a modeling study. J Geophys Res Oceans, 122(7): 6039–6054

Mellor G L, Yamada T (1982). Development of a turbulence closure model for geophysical fluid problem. Rev Geophys, 20(4): 851–875

Meng F, Dai M, Cao Z, Wu K, Zhao X, Li X, Chen J, Gan J (2017). Seasonal dynamics of dissolved organic carbon under complex circulation schemes on a large continental shelf: the northern South China Sea. J Geophys Res Oceans, 122(12): 9415–9428

Qiu D, Huang Y, Chen M, Guo Z (1985). Circulation structures in the studied waters. In: Comprehensive Investigations and Studies of the South China Sea II. Beijing: Science Press, 204–230 (in Chinese)

Reynolds R W, Smith T M, Liu C Y, Chelton D B, Casey K S, Schlax M G (2007). Daily high-resolution blended analyses for sea surface temperature. J Clim, 20(22): 5473–5496

Shaw P T, Chao S Y (1994). Surface circulation in the South China Sea. Deep Sea Res Part I Oceanogr Res Pap, 41(11–12): 1663–1683

Shi M C, Chen C S, Xu Q C, Lin H C, Liu G M, Wang H, Wang F, Yan J H (2002). The role of Qiongzhou Strait in the seasonal variation of the South China Sea circulation. J Phys Oceanogr, 32(1): 103–121

Shu Y, Chen J, Yao J, Pan J, Wang W, Mao H, Wang D (2014). Effects of the Pearl River plume on the vertical structure of coastal currents in the northern South China Sea during summer 2008. Ocean Dyn, 64 (12): 1743–1752

Shu Y, Wang D, Zhu J, Peng S (2011a). The 4-D structure of upwelling and Pearl River plume in the northern South China Sea during summer 2008 revealed by a data assimilation model. Ocean Model, 36(3–4): 228–241

Shu Y, Wang Q, Zu T (2018). Progress on shelf and slope circulation in the northern South China Sea. Sci China Earth Sci, 61(5): 560–571

Shu Y, Zhu J, Wang D, Xiao X (2011b). Assimilating remote sensing and in situ observations into a coastal model of Northern South China Sea using ensemble Kalman Filter. Cont Shelf Res, 31(6): S24–S36

Smagorinsky J (1963). General circulation experiments with the primitive equations, I. The basic experiment. Mon Weather Rev, 91 (3): 99–164

Song X, Lai Z, Ji R, Chen C, Zhang J, Huang L, Yin J, Wang Y, Lian S, Zhu X (2012). Summertime primary production in northwest South China Sea: interaction of coastal eddy upwelling and biological processes. Cont Shelf Res, 48: 110–121

Su J (2004). Overview of the South China Sea circulation and its influence on the coastal physical oceanography outside the Pearl River Estuary. Cont Shelf Res, 24(16): 1745–1760

Sun H L, Huang W M, Zhao J S (2001). Three-dimensional numerical simulation of tide-induced, wind-driven and thermohaline residual currents in the Beibu Bay. Oceanol Limnol, 32: 561–568 (in Chinese)

Wang D, Shu Y, Xue H, Hu J, Chen J, Zhuang W, Zu T T, Xu J (2014). Relative contributions of local wind and topography to the coastal upwelling intensity in the northern South China Sea. J Geophys Res Oceans, 119(4): 2550–2567

Wang D, Xu H, Lin J, Hu J (2008). Anticyclonic eddies in the northern South China Sea during winter 2003/2004. J Oceanogr, 64(6): 925–935

Wang D, Zhuang W, Xie S P, Hu J, Shu Y, Wu R (2012). Coastal upwelling in summer 2000 in the northeastern South China Sea. J Geophys Res, 117: C04009

Wang G, Su J, Chu P (2003). Mesoscale eddies in the South China Sea observed with altimeter data. Geophys Res Lett, 30(21): 2121–2126

Wang Q, Wang Y, Bo H, Zhou W, Wang D (2011). Different roles of Ekman pumping in the west and east segments of the South China Sea Warm Current. Acta Oceanol Sin, 30(3): 1–13

Wong L A, Chen J C, Xue H, Dong L X, Su J L, Heinke G (2003). A model study of the circulation in the Pearl River Estuary (PRE) and its adjacent coastal waters: 1. Simulations and comparison with observations. J Geophys Res, 108(C5): 3156

Wu C R, Shaw P T, Chao S Y (1998). Seasonal and interannual variations in the velocity field of the South China Sea. J Oceanogr, 54 (4): 361–372

Wu D X, Wang Y, Lin X P, Yang J Y (2008). On the mechanism of the cyclonic circulation in the Gulf of Tonkin in the summer. J Geophys Res, 113(C9): C09029

Wyrtki K (1961). Scientific results of marine investigation of the South China Sea and Gulf of Thailand. NAGA Report 2, 1–195

Xia H Y, Li S H, Shi M C (2001). Three-D numerical simulation of wind-driven current and density current in the Beibu Gulf. Acta Oceanol Sin, 20: 455–472

Xie J, Zhu J, Bertino L, Counillon F (2015). Analysis of the northern South China Sea counter-wind current in winter using a data assimilation model. Ocean Dyn, 65(4): 523–538

Xu X Z, Qiu Z, Chen H C (1982). The general descriptions of the horizontal circulation in the South China Sea. In: Proceedings of the 1980 Symposium on Hydrometeology of the Chinese Society of Oceanology and Limnology. Beijing: Science Press, 137–145 (in Chinese)

Xuan J, Huang D, Pohlmann T, Su J, Mayer B, Ding R, Zhou F (2017). Synoptic fluctuation of the Taiwan Warm Current in winter on the East China Sea shelf. Ocean Sci, 13(1): 105–122

Xue H, Chai F, Pettigrew N, Xu D, Shi M, Xu J (2004). Kuroshio intrusion and the circulation in the South China Sea. J Geophys Res, 109(C2): C02017

Yan C, Chen B, Yang S, Yan J (2008). The transportation volume of water through the Qiongzhou Strait in winter season. Transactions of Oceanology and Limnology, 1: 1–9 (in Chinese)

Yang H, Liu Q, Liu Z, Wang D, Liu X (2002). A general circulation model study of the dynamics of the upper ocean circulation of the South China Sea. J Geophys Res, 107(C7): 3085

Yang J (2007). An oceanic current against the wind: How does Taiwan Island steer warm water into the East China Sea? J Phys Oceanogr, 37 (10): 2563–2569

Zeng L, Wang D (2017). Seasonal variations in the barrier layer in the South China Sea: characteristics, mechanisms and impact of warming. Clim Dyn, 48(5–6): 1911–1930

Zeng L, Wang D, Chen J, Wang W, Chen R (2016a). SCSPOD14, a South China Sea physical oceanographic dataset derived from *in situ* measurements during 1919–2014. Sci Data, 3: 160029

Zeng L, Wang D, Xiu P, Shu Y, Wang Q, Chen J (2016b). Decadal variation and trends in subsurface salinity from 1960 to 2012 in the northern South China Sea. Geophys Res Lett, 43(23): 12181–12189

Zhang C, Ding Y, Bao X, Bi C, Li R, Zhang C, Shen B, Wan K (2017). A numerical study of the South China Sea Warm Current during winter monsoon relaxation. Chin J Oceanol Limnol, doi: 10.1007/s00343-018-6302-y

Zhang Z (2014). Observation and Analysis of the Coastal Current and Its Adjacent Current System in the China Offshore Waters. Dissertation for Ph.D Degree. Qingdao: Ocean University of China (in Chinese)

Zhang Z, Tian J, Qiu B, Zhao W, Chang P, Wu D, Wan X (2016). Observed 3D structure, generation, and dissipation of oceanic mesoscale eddies in the South China Sea. Sci Rep, 61, 24349

Zhu X H, Ma Y L, Guo X, Fan X, Long Y, Yuan Y, Xuan J L, Huang D (2014). Tidal and residual currents in the Qiongzhou Strait estimated from shipboard ADCP data using a modified tidal harmonic analysis method. J Geophys Res, 119(11): 8039–8060

Zu T, Gan J (2015). A numerical study of coupled estuary-shelf circulation around the Pearl River Estuary during summer: response to variable winds, tides and river discharge. Deep Sea Res Part II Top Stud Oceanogr, 117: 53–64

Zu T, Gan J, Erofeeva S (2008). Numerical study of the tide and tidal dynamics in the South China Sea. Deep Sea Res Part I Oceanogr Res Pap, 55(2): 137–154